Tampereen teknillinen korkeakoulu
Julkaisuja 388

Tampere University of Technology
Publications 388

Harri Vihriälä

Control of Variable Speed Wind Turbines

Tampere 2002

Tampereen teknillinen korkeakoulu
Julkaisuja 388

Tampere University of Technology
Publications 388

Harri Vihriälä

Control of Variable Speed Wind Turbines

Thesis for the degree of Doctor of Technology to be presented with due permission for public examination and criticism in Festia Small Auditorium 1, at Tampere University of Technology, on the 15th of November 2002, at 12 o'clock noon.

Tampere 2002

ISBN 952-15-0906-6 (printed)
ISBN 978-952-15-19 (PDF)
ISSN 0356-4940

TTKK-PAINO
Tampere, 2002

Abstract

Tampere University of Technology
Department of Electrical Engineering
Institute of Electromagnetics
Vihriälä, Harri: Control of Variable Speed Wind Turbines
Doctoral dissertation, 88 pages and 4 appendix pages
Advisors: Prof., Dr.Tech. Lauri Kettunen and Prof., Dr.Tech. Pertti Mäkilä
Funding: NEMO-programme of the Finnish Ministry of Trade and Industry, Centre for Technological Development (TEKES), Graduate School of Electrical Power Engineering, ABB Motors Oy, ABB Industry Oy, Fortum Oyj (Imatran Voima Oy), Neorem Magnets Oy (Outokumpu Magnets Oy), Teollisuuden Voima Oy, Finnish Cultural Fund, Ulla Tuominen Foundation and Jenny and Antti Wihuri Foundation
November, 2002
Keywords: wind power plants, wind turbines, nonlinear control, fuzzy control, Kalman filter, feed forward control, variable speed

A variable speed, fixed pitch wind turbine is difficult to control: it is stable at below rated wind speeds but becomes unstable as power output is limited by stalling the turbine at above rated wind speeds. This turbine is suitable especially for small, sub-100 kW wind power plants as we can avoid the use of a costly and failure-prone pitch mechanism.

The aerodynamic torque of the turbine is considered a disturbance to be cancelled by feedforward control. The torque cannot be measured and is estimated by a Kalman filter as an extended state. The estimated aerodynamic torque is also used to define a rotational speed reference and to restrict the power input. In addition, a fuzzy controller is designed and compared to a previous one. A turbine and wind field are modelled for the Kalman filter to operate.

The Kalman filter yields a good estimate of rotational speed from noisy measurement. In laboratory tests, both 100 kW and 300 W generators and frequency converters were subjected to variable wind torque. Both control algorithms, feedforward and fuzzy, operated satisfactorily. The tests showed that a Kalman filter must be used to give the fuzzy controller a good estimate of aerodynamic torque. Power output was controlled at all above-rated wind speeds. In the small turbine, maximum power was also restricted from 300 W down to 50 W without problems. The small wind turbine was also tested in a wind tunnel and in field conditions.

Tiivistelmä

Tampereen teknillinen korkeakoulu
Sähkötekniikan osasto
Sähkömagnetiikan laitos
Vihriälä, Harri: Muuttuvanopeuksisen tuulivoimalan säätö
Väitöskirja, 88 sivua ja 4 liitesivua
Ohjaajat: Prof., TkT Lauri Kettunen ja Prof., TkT Pertti Mäkilä
Rahoittajat: Kauppa- ja teollisuusministeriön NEMO-ohjelma, Teknologian kehittämiskeskus TEKES, Sähkövoimatekniikan tutkijakoulu, ABB Motors Oy, ABB Industry Oy, Fortum Oyj (Imatran Voima Oy), Outokumpu Magnets Oy (nyk. Neorem Magnets Oy), Teollisuuden Voima Oy, Suomen Kulttuurirahasto, Jenny ja Antti Wihurin rahasto ja Ulla Tuomisen säätiö
Marraskuu, 2002
Hakusanat: tuulivoimalat, epälineaarinen säätö, sumea säätö, Kalman-suodatin, adaptiivinen säätö, muuttuva pyörimisnopeus, myötäkytketty säätö

Tuulivoimala, jossa on muuttuvanopeuksinen turbiini ja kiinteä lapakulma, on vaikea hallita: Se on stabiili systeemi alle nimellisella tuulennopeudella ja epästabiili nimellisen ylittävillä tuulennopeuksilla. Tämäntyyppinen turbiini on kuitenkin käyttökelpoinen pienissä, alle 100 kW:n laitoksissa, sillä silloin vältytään kalliilta ja vikaantumisherkältä lapakulmansäätömekanismilta.

Aerodynaminen momentti käsitetään häiriöksi, jonka vaikutus eliminoidaan myötäkytketyllä säädöllä. Tätä momenttia ei voida mitata ja siksi se estimoidaan turbiinin ylimääräisenä tilana. Estimoitua aerodynaamista momenttia käytetään myös pyörimisnopeusohjeen määrittelyssä ja tehonrajoitukseen. Sumea säätäjä on myös suunniteltu ja verrattu myötäkytkettyyn. Turbiini ja tuulet turbiinin alueella on mallinnettu, jotta Kalman-suodin voisi toimia.

Kalman-suotimella saadaan myös hyvä estimaatti todellisesta pyörimisnopeudesta häiriöllisestä mittauksesta huolimatta. Testipenkissä sekä 100 kW:n ja 300 W:n generaattorit suuntaajineen altistettiin tuulen vaihtelevalle momentille. Molemmat säätömenetelmät toimivat tyydyttävästi. Kalman-suotimen antamaa estimaattia aerodynaamisesta momentista tarvitaan sittenkin myös sumeassa säädössä. Tuulesta otettu teho saatiin rajoitettua aina kun tuulennopeus oli yli nimellisen. Pienellä tuulivoimalalla annettua tehoa rajoitettiin 300 W:sta 50 W:in vaikeuksitta. Pientä tuulivoimalaa testattiin myös tuulitunnelissa ja kentällä.

To Viola and Daniel, with love

The whole man must move at once.
-Hugo von Hofmannsthal:
Die Briefe des Zurückgekehrten

Preface

Lic. Tech. Lasse Söderlund took over this project after Professor Eriksson was voted rector, and I thank Lasse for his good companionship, instruction, and advice on my work.

I also thank Professor Lauri Kettunen for advising my thesis and setting high standards for reseach at the Institute. I had many good discussions with my third advisor Prof. Dr. Tech. Pertti Mäkilä, of which I am grateful. Furthermore, M. Sc. Erkki Haapanen advised me many times on aerodynamics.

I thank Lic. Tech. Raine Perälä, who did a tremendous job designing, building, and testing the 5, 10, and 100 kW permanent magnet generators. After I had had the idea to use a current-source frequency converter with a permanent magnet wind generator to bring down the number of active components, Lic. Tech. Pasi Puttonen from the Laboratory of Power Electronics designed, built, and tested the current-source generator.

Mr. Matti Hyppönen initiated the program for the small generators, manufactured their parts, and provided splendid facilities for field testing. Also Matti and Lic. Tech. Heikki Laine participated in this testing and generously offered their valuable experience and skills many times during the project. M. Sc. (E.E.) Teemu Rovio designed the small permanent magnet generators while M. Sc. (E.E.) Mr. Jarmo Kriikka designed and built their control electronics and programmed the microcontroller, including the control algorithms and the Kalman filter under the author's ofttimes garbled guidance. M. Sc. (E.E.) Pasi Ridanpää designed and simulated the fuzzy control system. I thank these gentlemen for their gracious help.

I thank our secretary Mrs. Maija-Liisa Paasonen for the office work she did for me and for her secretarial assistance and Mrs. Heidi Koskela for drawing the professional illustrations in this thesis. Thanks are also due to Dr. Timo Lepistö for proofreading the English of the work.

I thank the staff at the Institute of Electromagnetics for providing such a good and high-level working atmosphere, including our recreational activities. However, let the record show that thanks do not cover the boring Tyrvää tales told by Dr. Tech. Jorma Lehtonen. I also wish to honor our good suppliers, who put their extensive selections at our disposal, Biltema and Rauta-Soini Oy among others.

I thank the staff at Institute of Power Electronics, especially Prof. Dr. Tech. Heikki Tuusa, and Lic. Tech Mika Salo for their assistance and cooperation.

My reseach was funded by the NEMO-programme of the Finnish Ministry of Trade and Industry, the Centre for Technological Development (TEKES), the Graduate School of Electrical Power Engineering, ABB Motors Oy, ABB Industry Oy, Fortum Oyj (Imatran Voima Oy), Neorem Magnets Oy (Outokumpu Magnets Oy), Teollisuuden Voima Oy, the Finnish Cultural Fund, the Ulla Tuominen Foundation, and the Jenny and Antti Wihuri Foundation. All their support is gratefully acknowledged.

I thank my family, my parents, and my late grandmother for their love and support. My wife Bea I thank for her love and patience and Viola and Daniel for their impatience. You managed to make me forget the work at times and concentrate on other important things in life.

Contents

List of Figures

List of Tables

List of symbols and abbreviations

A	state transformation matrix
A_f	Kalman filter state transformation matrix
A_{gap}	Kalman filter state transformation matrix
A_{turb}	area of turbine
A_w	Weibull scale parameter
a, a_i	constant
B	input matrix
$B_{bearings}$	frictional coefficient of bearings
B_{drive}	frictional coefficient of test bench
B_f	Kalman filter input matrix
B_g	frictional coefficient of generator
B_{gap}	Kalman filter input matrix
B_{seals}	frictional coefficient of seals
B_t	frictional coefficient of turbine
$B_{t,sim}$	frictional coefficient of turbine, simulated
B_{total}	total frictional coefficient of drive train
b	width of wing section
b_c	constant
C	output matrix
C_{gap}	output matrix
C_f	Kalman filter output matrix
C_{Q}	torque coefficient of turbine
C_0, C_1, C_2	constants
c	apparent air flow

c_A axial thrust coefficient of blade profile

c_D drag coefficient of blade profile

c_L lift coefficient of blade profile

c_{opt} optimal power coefficient of turbine

c_{P} power coefficient of turbine

$c_{\mathrm{P},0}$ power coefficient of turbine at optimal operating point

c_{T} torque coefficient of turbine

D input matrix

D_f Kalman filter input matrix

E_t energy extracted by turbine

E_w energy of wind

e_{ab} tracking error, above rated

e_{be} tracking error, below rated

e_1, e_2 tracking error

F_A axial force of wind

F_{base} pressure force of air

F_D drag force on wing section

F_L lift force on wing section

F_R braking force on wing section

F_{thrust} thrust force of wind

f frequency

H reference height

h sample time

G_{ra} transfer function of rotor area

I identity matrix

$I_{a,ref}$ generator current reference

$I_{battery}$ battery current

I_{dc} DC current

$I_{dc,ref}$ DC current reference

I_{grid} grid current

I_t transfer function of induction lag

J_d inertia of drive train

J_g inertia of generator

J_t inertia of turbine

$J_{t,sim}$ inertia of turbine, simulated

J_{total} total inertia

K gain matrix

K_f Kalman filter gain matrix

K_k diagonal gain matrix

K_p proportional part of PID controller

K_v constant

k time (discrete)

k_T constant of turbine

k_ω constant of turbine

k_w Weibull form factor

L body length

m Gaussian white noise

n constant

n_{sync} synchronous rotational speed

P power

P_a	aerodynamic power
P_{grid}	power fed to the grid
P_{max}	maximum power
P_n	rated power
P_{turb}	power produced by turbine
P_{wind}	power in wind
P_x	covariance matrix
P_2	constant
p	number of pole pairs
Q_1	weighting parameter for state in LQ/LQG control
Q_2	weighting parameter for control in LQ/LQG control
R	radius of turbine
Re	Reynolds number
R_1	system error covariance matrix
R_2	measurement error covariance matrix
T	torque
T_a	aerodynamic torque
$\hat{T}_a$	estimated aerodynamic torque
ΔT_a	deviation from linearised aerodynamic torque
$T_{a,opt}$	optimal aerodynamic torque
$T_{ab,ref}$	above rated reference torque
$T_{be,ref}$	below rated reference torque
T_f	frictional torque
T_g	generator torque
ΔT_g	change in generator torque

T_{gap}	torque gap between $T_{g,ref}$ and T_g
$T_{g,0}$	generator torque at linearization point
T_{max}	maximum torque
T_L	time constant of aerodynamic torque
T_{ref}	torque reference
T_v	constant
T_1	torque limit
T_2	torque limit
t	time (continuous)
$U_{battery}$	battery voltage
U_{dc}	DC voltage
U_{grid}	grid voltage
u	input, continous time
u_k	input, discrete time
v_{cut-in}	cut-in wind speed
v_n	nominal wind speed
$v_{cut-off}$	cut-off wind speed
v_t	wind speed
Δv_t	change in wind speed
$v_{t,lin}$	wind speed, linearised
$v_{t,0}$	base wind speed for linearization
v_0	reference wind speed
w	Weibull distribution
v_1	system error
v_2	measurement error

w_k discrete measurement noise

x state vector

$\hat{x}$ estimated state vector

x_k state vector, discrete time

$\hat{x}_k$ estimated state vector, discrete time

x_0 state vector at reference point

z height above terrain

z_b number of blades

z_0 roughness length

Greek symbols

α angle of attack

β pitch angle

β_{ref} pitch angle reference

β_s spatial filter constant

β_0 pitch angle at linearised operating point

γ aerodynamic damping coefficient, derivative of T_a w.r.t. β

ε weighting factor

ε_{glide} glide number

η measurement noise

θ derivative of T_a w.r.t. x_0

θ_{drive} angular position

θ_{ref} angular position reference

κ derivative of T_a w.r.t. ω_t

λ tip speed ratio of turbine

λ_{opt} optimal tip speed ratio

λ_0 tip speed ratio of turbine at linearised operating point

ξ variance of aerodynamic torque

ρ air density ($\sim$ 1,26 kg/m^3 in standard atmosphere at 20 °C)

$\sigma_{v,lin}$ turbulence intensity

τ_i time constant of induction lag

Φ_v spectral density

ϕ angle between voltage and current

ϕ_d decay factor

ω frequency

ω_c constant rotational speed

ω_g rotational speed of generator

ω_{max} maximum rotational speed

ω_{min} minimum rotational speed

ω_{opt} optimum rotational speed

ω_{ref} rotational speed reference

ω_t rotational speed of turbine

$\hat{\omega}_t$ estimated rotational speed of turbine

$\omega_{t,0}$ rotational speed of turbine at linearised operating point

Abbreviations

AC alternating current

C_I current controller

C_{pitch} controller of pitch angle

C_ω controller of rotational speed

C_θ	position controller
CE	change in error
CFD	computational fluid dynamics
CS	current source
DC	direct current
DU	change in control
E	error
FC	frequency converter
FET	field effect transistor
FSFP	fixed speed-fixed pitch
FSVP	fixed speed-variable pitch
G	generator
IGBT	insulated gate bipolar transistor
LQG	linear quadratic Gaussian (control)
MIMO	multiple input-multiple output
O.P.	operating point
PC	personal computer
PI	proportional-integrator
PMG	permanent magnet generator
PMW	pulse width modulation
SISO	single input-single output
TUT	Tampere University of Technology
VSFP	variable speed-fixed pitch
VSVP	variable speed-variable pitch
WT	wind turbine
w.r.t.	with respect to

Chapter 1

Introduction

Depletion of fossil fuels and the concomitant climate change have compelled nations to seek new, nonpolluting ways to produce energy. Consequently, "new," renewable energies like wind, solar, biomass, and geothermal energies have been viewed as attractive solutions. The use of wind power has indeed been on the rise: by the end of 2001, over 24 GW of wind power capacity was installed in the world, an increase of 6 GW in 2001 alone [45]. In the period 1991-2001, the wind turbine markets saw a rapid growth of an average of 40% per year, and in this slowly-growing power industry such growth was very high indeed. The countries with the most wind power penetration are Germany (10 GW; 3.5% of the electricity consumed over a normal wind year), Spain (3.3 GW), Denmark (2,4 GW; 18%), USA (1.7 GW), and India (1.4 GW). The wind industry employs approx. 30,000 people in Germany and 20,000 in Denmark, including subcontractors. Finland has a wind power capacity of only 43 MW (0,1% of the consumption). However, in 2002, Finnish exports of wind power plant components are estimated to exceed 200 Million Euros and employment in the industry 1,000 people. The growth is estimated to continue by at least 16% per year, which is a high growth rate in the energy sector.

Much of the current wind power capacity consists of windmills built according to the so-called Danish concept, which relies on crude but reliable technology. However, as wind power plants grew in size (up to 1.5 MW and above), it became clear that more sophisticated technologies were needed to reduce the weight and cost of the main components. One such technology is to use variable speed. As the power electronics decouple the turbine's rotational speed from the grid frequency, power spikes from gusts are not transferred into the grid, some stresses are minimized on the blades and the drive train, and the energy production of the plant is increased by 6-15% [78]. In addition, as the gearbox and other drive train components do not

have to be overdimensioned, costs of the components can be brought down.

At low wind speeds the variable speed wind turbine, accordingly, rotates more slowly, thereby cutting down noise from blade tips, in comparison to fixed speed drives. With variable speed, we can also use several different control strategies in different sites. For a similar wind turbine in different wind conditions, a variable speed drive offers greater flexibility over a fixed speed drive.

Another reason for using variable speed is pitch control, which was introduced to relieve windwise loads on the tower. In practice, with pitch control, variable speed is needed to dampen the power peaks by gusts in the above rated wind speed region. In sub-100 kW wind turbines, pitch control is too expensive and prone to failure; therefore, the turbines are equipped with fixed-pitch blades. Hence the only control input is generator torque.

Variable speed, fixed pitch (VSFP) turbine is mechanically less complex but theoretically more so. The stalling of the blades limits power output and destabilizes the turbine. A control system is thus needed to stabilize it over the whole operating region. A second important task for the control system is to regulate the power extracted from the wind. At below-rated wind speeds, power output is maximized and at above-rated wind speeds kept at a nominal value.

In general, long time constants result in slow behavior [25], which makes it easier to control the VSFP wind turbine. The literature has very little to say about this type of plant, as most nonlinear plants are stable at all operating points. The control task is even more difficult, since the wind speed cannot be measured accurately. Accordingly, a drive with fixed blades and variable speed clearly needs a new controller to operate at all.

The optimal strategy for the below-rated wind speed region was introduced by Buehring [10] in 1981. Since the plant is stable in this region, it can be controlled by a single proportional (P) controller. Control strategies for both the below- and above-rated region as well as the intermediate region were studied by Leithead and Connor [14], [15], [36], [37], [38].

In their control strategy, Leithead and Connor proposed a robust two-level controller [16]. Robb designed a model-based predictive control algorithm [63], which contains also a feedforward part. Ekelund and Novak studied linear quadratic gaussian (LQG) control of a fixed-pitch, variable speed wind turbine [19], [54], [53]. In his doctoral thesis, Ekelund regarded aerodynamic torque as a disturbance, made up of a linear combination of rotational speed and wind speed, and estimated it to be an additional state [20]. Bongers reported on the modeling and control of a variable speed-variable pitch (VSVP) wind turbine [7], [8], which applies well to fixed pitch machines.

1.1 Motives of this research

This research had its start as a part of a permanent magnet generator project at the Institute of Electromagnetics at Tampere University of Technology (TUT). In 1993, a project was launched on gearless permanent magnet generators for wind power plants. The first topology to be studied was the axial flux machine with a toroidal stator winding (Fig. 1.1). These machines are comparable to synchronous machines with constant excitation. In wind power applications, the turbine rotates at low a speed and requires high torques for a given generator rating. Axial flux machines have higher torque/volume and torque/weight ratios than radial flux machines, which makes them an attractive alternative for wind power drives.

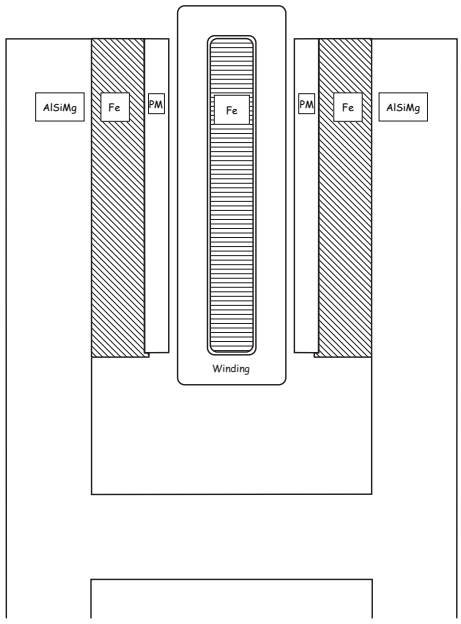

Figure 1.1: Cross section of a large axial permanent magnet generator

The topology was tested first with a 5/10 kW model generator, and later a 100 kW, 2,5-m diameter generator (G) was built. Furthermore, several small permanent magnet generators with ratings of 300-400 watts were built. Because of the gustiness of winds synchronous machines cannot be directly connected to the grid. Therefore, they were connected via a frequency converter (FC; Fig. 1.2). The FC allows us to regulate the rotational speed within a broader area and thus ensure operation at the highest turbine efficiency. In smaller generators, the electricity produced was rectified in a

controlled manner, but the same conditions apply here as in large generators.

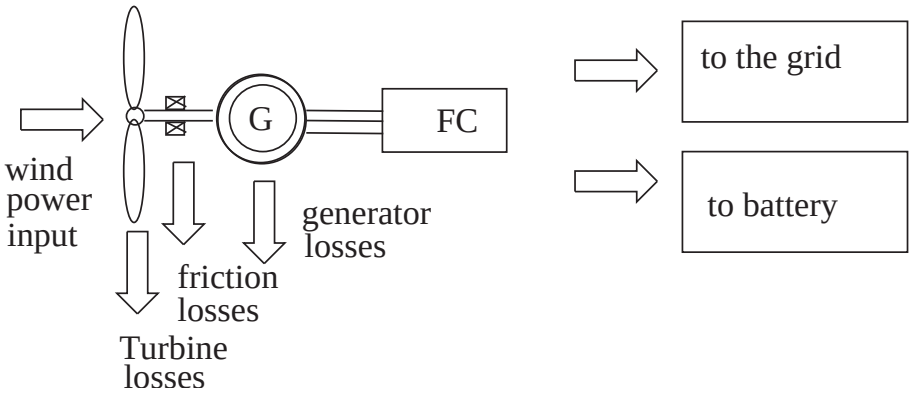

Figure 1.2: Schematics of different systems

1.2 Objectives of this research

The main objective was to design a controller that would ensure stability and optimal operation of a variable speed, fixed pitch turbine at all operating points. The turbine had to be modeled in order to test the designed controller by simulation and laboratory tests. The designed controller was to be tested in real wind power drives, both large and small. For both drives, a simple, economically viable drive was sought.

As mentioned earlier, Ekelund used aerodynamic torque as a state in LQG control. I came up with the idea of feeding aerodynamic torque forward into generator torque to cancel its dynamic effects. The feedforward control structure is used in a similar fashion in robotics (and called there the joint torque feedback) to combat load changes, mismodeling of robot dynamics, and nonlinearities of the system. The application in robotics can be regarded as a special case of Ekelund's LQG control design.

The wind turbine is modeled and simulated with simple models. Aerodynamic torque is estimated by a Kalman filter, whose inputs are generator torque and measured rotational speed and which then returns an estimate of aerodynamic torque and rotational speed. The rotational speed reference is also determined by aerodynamic torque. Rotational speed is controlled by various controllers, including proportional, feedforward, and fuzzy controllers.

I found out how aerodynamic power input can be restricted below the nominal with the outermost control loop. Therefore, torque, rotational speed, and power output can all be controlled with the generator current alone. This thesis concentrates on the control of the variable speed drive with direct-driven generators, but its findings can also be applied to drives equipped with gears, other types of generators, or even hydraulic (hydro-dynamic) transmissions, as long as they operate under variable speed.

I also designed classical control systems and tested all the control systems. These designs have been extensively simulated and tested on laboratory benches with both large (100 kW) and small (300 W) wind turbine drives.

1.3 Organisation of the thesis

Chapter 2 introduces the energy distribution of wind and briefly the wing section theory to highlight the importance of variable speed. An appropriate strategy for rotational speed control is proposed. Chapter 3 discusses the advantages and disadvantages of variable speed in wind turbines and how it could be realized. Chapter 4 describes modeling of wind in the turbine disk and modeling of a wind power drive. Chapter 5 introduces design of the speed control loop for gain scheduled, feedforward, and fuzzy controllers. Chapters 6 and 7 discuss tests of large and small drives and control algorithms. Test drive parameters are identified first and then elaborated on the problems and results. Chapter 8 provides conclusions and topics for further research.

Chapter 2

Control of wind turbine

In this chapter, the energy content of wind is studied and why it is important to be able to control the power output of wind. Then, the objectives of wind turbine control are presented. In the last section, a wing section theory is examined briefly for wind turbines to show how aerodynamic forces are generated in wind turbines.

2.1 Energy distribution of wind

The power of wind is proportional to wind speed cubed:

$$P_{wind} = \frac{\rho}{2} A_{turb} v_t^3, \tag{2.1}$$

where ρ is the density of air (approx. 1.26 kg/m^3 in standard atmosphere at 20°C), A_{turb} the area of the turbine perpendicular to the wind direction and v_t wind speed. According to Betz [4], an ideal wind turbine would in theory extract the 16/27:th (0.5925) part of this power. If we maximised the force of air, air velocity would drop to nil on the rotor plane, i.e., air flow would totally cease. Similarly, if we maximized the velocity of air (i.e. did not decelerate it at all), its force would be nil. In both cases power would be zero. By decelerating the velocity of air flow by 2/3, the above optimum extraction is achieved. Non-homogeneous flow and friction reduce the extracted power to about a half of the power of wind.

Because of the design and sites of wind turbines, we are interested in the energy content of wind on a given site and its wind speed distribution. The energy content determines whether it is worthwhile building a turbine on the site, and the energy distribution provides us with information about the prevalent wind speeds to help us design a wind turbine.

A standard method to determine wind speed distribution is to measure 10 minute average values with an anemometer. The wind speed distribution at a given point can be given by using the Weibull distribution:

$$w(v_t, A_w, k_w) = \frac{k_w}{A_w^{k_w}} v_t^{k_w - 1} e^{-(\frac{v_t}{A_w})^{k_w}}, \tag{2.2}$$

where A_w is the scale parameter and k_w the form factor, which usually equals 2.

If only a median wind speed, v_m, and the form factor are given, then the Eq. (2.2) reads as [26]

$$w(v_t, v_m, k_w) = v_m^{-k_w} \log(2) k_w v_t^{k_w - 1} e^{-\log(2)(\frac{v_t}{v_m})^{k_w}}. \tag{2.3}$$

As we multiply the wind speed distribution in Eq. (2.2) by the power of wind (2.1), we get the energy distribution of the wind (Fig. 2.1), which tells us clearly that wind energy is widely distributed on a single site. Finally, the total energy content of the wind can be integrated as

$$E_w = \int_0^\infty w(v_t, A_w, k_w) P_{wind}(v_t) dv_t. \tag{2.4}$$

As we examine the distributions of wind and energy, we see little energy production at both ends of the speed distribution: light wind speeds are prevalent and produce little power and stormy winds occur seldom and for a short duration.

The energy distribution affects profoundly the specifications of the wind power plant, as the plant should be as efficient as possible in the region of most energy contents. This efficiency, however, is compromised by economic factors. One example is the power rating of wind turbines. As nominal power is reached, part of the extractable wind energy must be discarded. Therefore, wind power plants reach their nominal power at the right end of the energy distribution, at 12-15 m/s.

Wind turbines should also accommodate varying energy distributions on different sites, such as a sea shore versus an inland site. In some cases, we can do this by changing the size of the turbine and the nominal and cut-off wind speeds. But this variation is also restricted by economic considerations, for on poor sites (below 5 m/s average wind speed), the energy produced is too little to repay the investment, whereas wind sites with very good wind regimes may be too few to justify the cost of designing a separate model for the sites, as the energy yield on the sites is abundant enough with suboptimal power plants. On Finnish inland sites, the energy calculated by the Weibull distribution is 10% higher than that given by measurements [73].

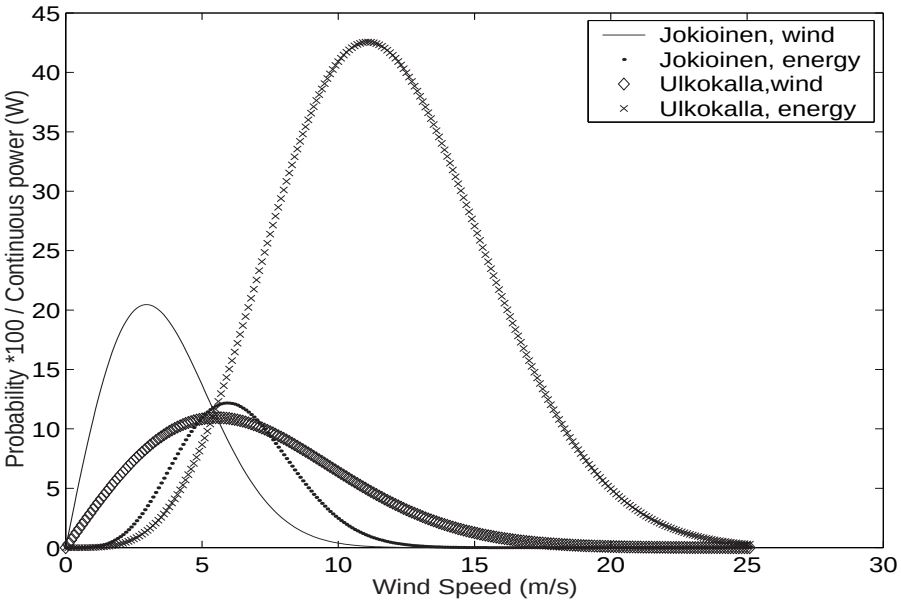

Figure 2.1: Wind speed and energy distributions in two different wind regimes: fair (Jokioinen, 3,8 m/s median wind speed) and very good (Ulkokalla, 7,0 m/s)

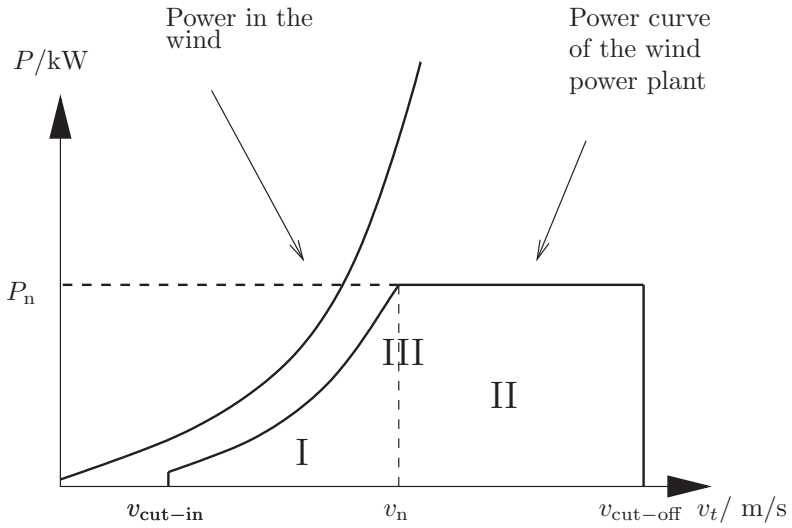

Figure 2.2: Different regions of wind turbine control

The control of a wind turbine constitutes three distinct areas, as shown in Fig. 2.2.

I $[v_{\text{cut}-\text{in}} \dots v_n]$ Maximization of extracted energy: the wind turbine should extract wind energy at the highest efficiency.

II $[v_{\text{n}} \dots v_{\text{cut}-off}]$ Limitation of extracted energy: the controls aim primarily to limit stresses and secondarily to minimize the power fluctuations around a constant value, normally the nominal power P_n.

III $[v_n]$ Determination of the operating point and the decision, accordingly, as to which control strategy to adopt.

2.2 Objectives of wind turbine control

The objectives of wind turbine control were quite pre-emptively defined by Leithead et al. in [37] as follows:

- to maximise the energy yield of wind by tracking closely the tip speed ratio at the point where the power coefficient is at maximum
- to reduce the variation of torque peaks generated by wind gusts and thus to minimize both stress on the mechanical parts of the wind turbine and power fluctuations in the grid

- to limit the power extracted from wind to the nominal value of the wind turbine
- to reduce drive-train transients
- to minimize control action
- to stabilize the system under all operating conditions
- to suppress those frequencies which may cause resonance in the mechanical structure

Wobben presented one more auxiliary criterion [81]:

- to control grid voltage and power by regulating the output of the wind turbine

2.3 Means of wind turbine control

Wind turbines consist (usually) of three aerodynamically designed blades. The cutout of these blades is an aerodynamic profile, which induces aerodynamic lift and drag as the blade profile encounters air flow (at a radius of R and a pitch angle of β, while the turbine is rotating at a speed of ω_t; see Fig. 2.3). Lift (F_L) is a force perpendicular to the direction of the flow and drag (F_D) in the parallel direction. Lift and drag vary according to the (relative) speed of air flow, dimensions of the wing, density of the air, and the angle between the chord line and speed vector of the flow. This angle is called the angle-of-attack, α. The forces of lift and drag for a body length of L and a width of b in flow with a speed of c and a density of ρ are given by

$$F_L = c_L(\alpha)\frac{\rho}{2}c^2Lb \tag{2.5}$$

$$F_D = c_D(\alpha)\frac{\rho}{2}c^2Lb. \tag{2.6}$$

For a given profile, a coefficient can be obtained for lift (c_L) and drag (c_D) as a function of the angle of attack in wind tunnel tests or now also by computer, based on analytical formulations or computational fluid dynamics (CFD) [55]. The $c_L(\alpha)$ and $c_D(\alpha)$ curves depend on the Reynolds number, Re, which relates blade dimensions to flow speed as

$$Re = 68460 \cdot c \cdot L \tag{2.7}$$

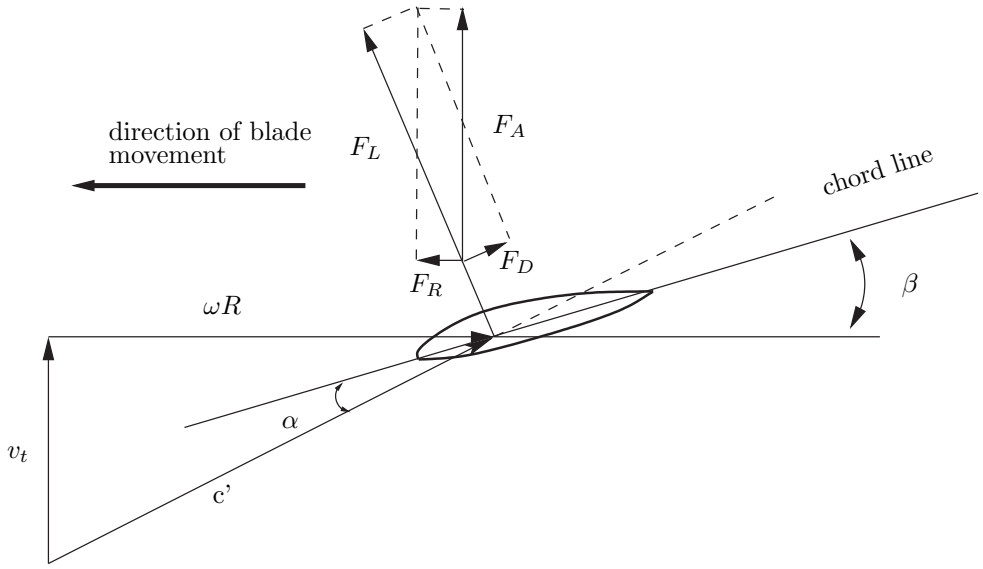

Figure 2.3: Forces on wind turbine blade section

which applies to a body in free, uncompressed flow. As Re drops below the critical values (ca. 100 000 -200 000; depending on profile shape [24]), the characteristics of the profile become significantly worse, a fact which is important in designing small wind turbines. The blade of a wind turbine is designed with the angle α, which maximizes the glide number

$$\varepsilon_{glide}(\alpha) = \frac{c_L(\alpha)}{c_D(\alpha)}, \tag{2.8}$$

i.e., the maximum amount of lift is created with minimum drag. Since $\omega_t R$ and v_t vary along the radius, so do also the twist angle and chord length [24]. Different profiles are used for different radial positions of the blade (NACA xxxx, NACA 6-digit, laminar or special profiles designed for wind turbines).

In an ideal wind turbine, lift and drag vectors are mapped to the axis along the turbine shaft and along the turbine radius, resulting in axial F_A and radial F_R forces (Fig. 2.3). We have two ways to control the wind turbine by changing the angle of attack, α: by changing the pitch angle β or by controlling its rotational speed. The former method is called pitch control, whereas the latter is done by varying generator torque on the turbine shaft, i.e., via variable speed control, which changes the length of the speed vector $\omega_t R$ and thus the apparent air flow vector c, which in turn affects the angle of attack α. In Fig. 2.3, these vectors are shown in the right proportion to each other. $\mid \omega_t R \mid$ has typically the values of 4–8$\cdot|v_t| = \lambda \cdot |v_t|$, and α

is typically 5–15° in the below-rated power region. λ is the tip speed ratio, which is defined by

$$\lambda = \frac{\omega_t R}{v_t}. \tag{2.9}$$

We can sum up the axial and perpendicular components along the blade to obtain aerodynamic torque and thrust for the whole turbine.

$$T_a(v_t, \omega_t) = z_b \int_R r F_R(v_t, \omega_t) dr \tag{2.10}$$

$$F_{thrust}(v_t, \omega_t) = z_b \int_R F_A(v_t, \omega_t) dr, \tag{2.11}$$

where z_b is the number of blades. The above can be calculated at various wind speeds. To normalize the data base obtained, T_a and F_{thrust} can be divided by the pressure force of air, $F_{base} = \frac{\rho}{2}\pi R^2 v_t^2$. Hence we obtain the dimensionless torque and axial thrust coefficients, c_T and c_A. The data can be generalized even further if we use the tip speed ratio, resulting in

$$c_T(\lambda) = \frac{T_a(v_t, \omega_t)}{R F_{base}(v_t)} \tag{2.12}$$

$$c_A(\lambda) = \frac{F_{thrust}(v_t, \omega_t)}{F_{base}(v_t)}. \tag{2.13}$$

Consequently, we obtain the dependencies of c_T and c_A at different wind speeds and rotational speeds. With small turbines, these curves differ at the near- and below-critical Reynolds number. If we multiply the torque coefficient by the tip speed ratio, we obtain the power coefficient

$$c_P = c_T \cdot \lambda, \tag{2.14}$$

which describes the efficiency of the turbine. It is clear that to maximize the energy of wind, the turbine should be operated near the peak of the c_P-curve. Fig. 2.4 shows power and torque coefficient curves for different turbines. One- to three-blade turbines used to rotate generators show clearly good efficiencies at high rotational speeds, whereas multiblade turbines running pumps and sawmills turn more slowly but have high starting torques at $\lambda = 0$.

It should be noted that no stall-delay is considered in Fig. 2.4 : c_P, c_T-curves are dynamically valid (which may not be true in the stall transition region).

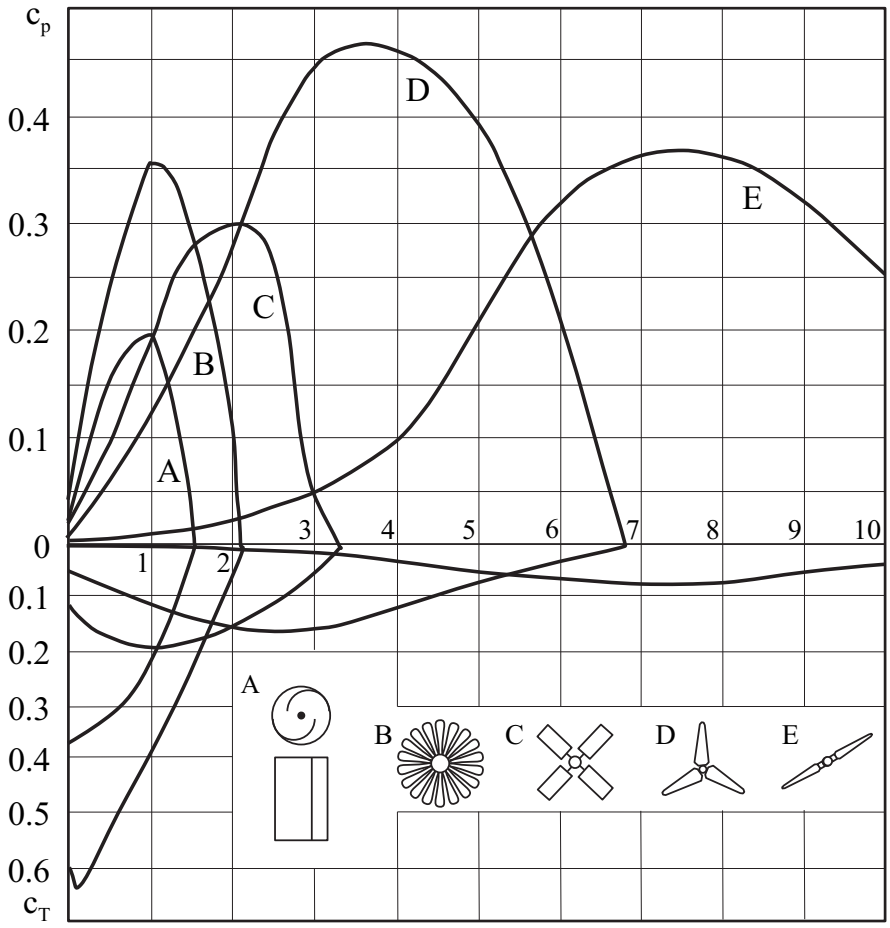

Figure 2.4: Power (c_P) and torque coefficient (c_T) versus tip speed ratio (λ) for different turbines [22]

Chapter 3

State of the art in variable speed drives

3.1 Why variable speed

Wind energy is distributed over a wide range of wind speeds. Additionally, the turbine should perform well over a wide range of sites in different wind conditions without extensive modifications. However, the wind turbine with fixed rotational speed works at its highest efficiency only within a narrow range of wind speed, as seen in Fig. 2.4. Therefore, it seems obvious that to maximize the efficiency of the turbine, we should be able to vary its rotational speed.

However, when the wind reaches the speed rated for the turbine, the power of the turbine should be restricted, i.e., c_P should be lowered. We should not allow the tip speed ratio to increase, because the turbine would then overspeed and become dangerous owing to the amount of energy stored in the rotating mass, vibration problems, and increased axial forces.

The energy production of the wind turbine can be obtained by Eq. (2.4) if the wind power $P_{wind}(v_t)$ is replaced by the power curve of the turbine $P_{turb}(v_t)$

$$E_t = \int_0^\infty w(v_t, A_w, k_w) P_{turb}(v_t) dv_t. \tag{3.1}$$

The energy production of variable, fixed speed, and two-fixed-speeds drives was compared in the same turbine in [78]. The power coefficient curve of the turbine is shown in Fig. 3.1. The variable speed, gearless permanent magnet generator (PMG) drive produced 5-10% more energy than the fixed speed drive with two speeds, or 10-15% more than the single speed drive (both had an asynchronous generator with a gearbox). Energy productions

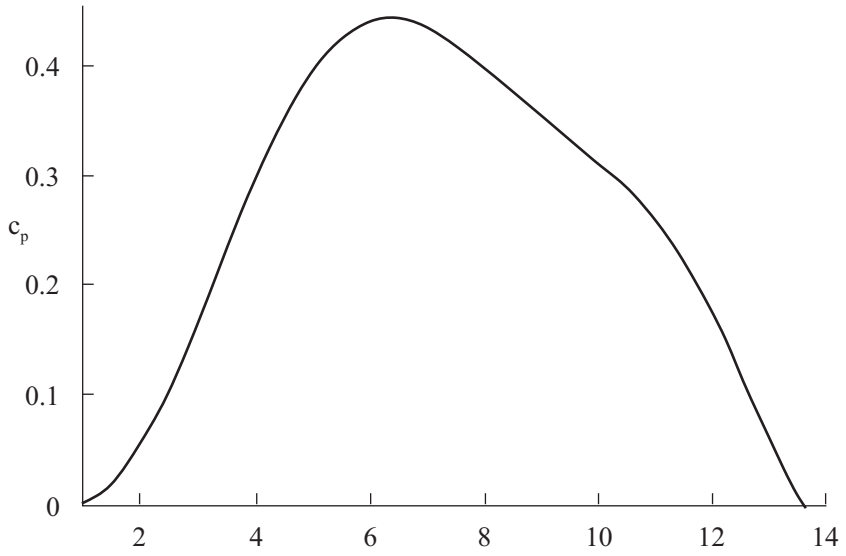

Figure 3.1: Power coefficient (c_P) versus tip speed ratio (λ) for a three bladed turbine in [78]

relative to the single speed drive are shown in Fig. 3.2 as a function of rated wind speed. This difference alone does not justify using the variable speed drive, if we take into account also increased costs and the added complexity of the drive.

For twenty years between 1979-1999, most commercial wind turbines were built according to the so-called Danish concept, a fixed-speed, stall-regulated wind turbine. As wind turbines grew in size to 600 kW and above, the Danish concept was no longer economical, because high thrust loads (in blades: flap loads) at above-rated wind speeds required heavy support structures. Consequently, the tower and the machine bed had to be strengthened to sustain high loads. Also the grid suffered from high power peaks.

If the turbine has pitch control, we can obtain multiple c_T, c_P, and c_A -curves. The pitch angle β is increased and the attack angle, α, decreased with the point of operation moving lower on the c_T-curve, as shown in Fig. 3.3. However, pitch control combined with fixed speed caused even more power peaks in the grid, because at above-rated wind speeds, pitch control operates on the c_T -curve with higher $\partial c_T/\partial v_t$ values [47]. Therefore, we needed variable speed to dampen the power peaks and to let the turbine accelerate and store energy in it during gusts. This is another important task for variable speed: to dampen torque peaks caused by wind gusts. We can achieve this by letting the rotational speed vary a few percent around a fixed value.

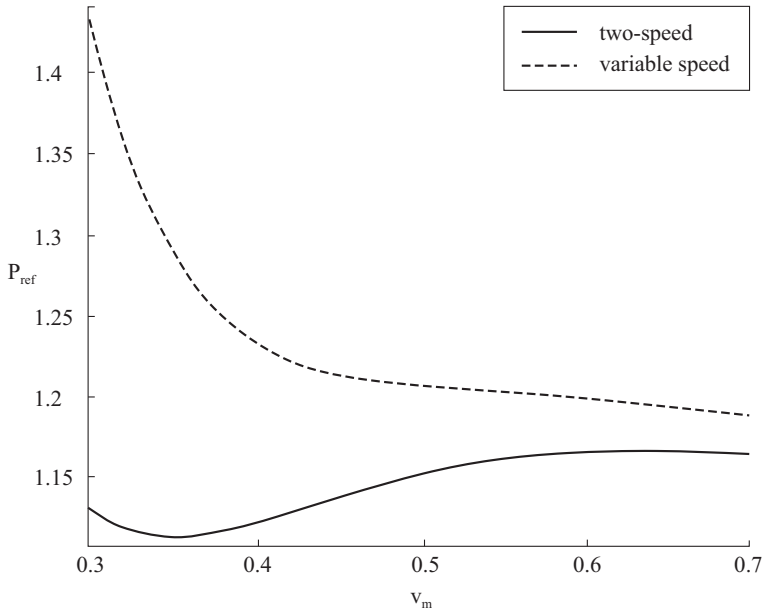

Figure 3.2: Relative power production, P_{ref}, of a two-speed and a variable speed wind turbine. v_m is median wind speed, normalized by rated wind speed v_n

Technical solutions to realize variation of rotational speed were discussed in [75]. The most common solution is the so-called Optislip (TM) technique, invented by the Danish Vestas [1]. An asynchronous generator with a wound rotor is used in this application, and the resistance of the rotor windings can be varied with power electronics and an additional resistor, attached to the rotor, as shown in Fig. 3.4. This way the slip of the generator can be varied momentarily and its rotational speed increased by 10% during gusts. Another means to dampen torque peaks is to attach a fluid coupling between turbine and generator (hydro-static coupling) or to mount the generator in a flexible manner.

The turbine can also be pitched by decreasing the β angle to assist the blade to stall, a concept named Active Stall by the wind turbine manufacturer Bonus [72]. Active stall is used in conjunction with fixed speed wind turbines (WTs), and it has the advantage of shorter pitching angles. It also compensates for the effect of colder, i.e., denser air and dirty blades, for the average power can be restricted to nominal. However, the problem of power peaks fed into the grid, high windwise loads plus other fixed speed problems remain.

One method to restrict power extraction from wind is to keep the rota-

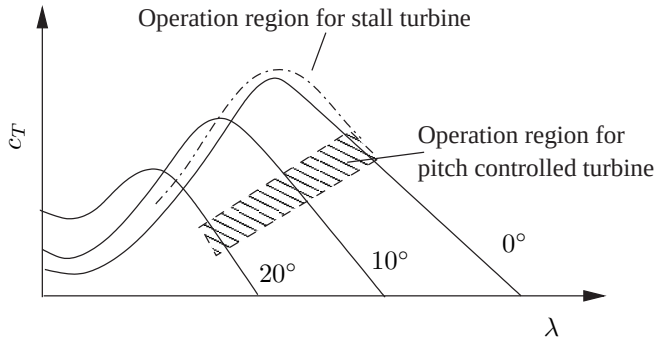

Figure 3.3: Comparison of pitch and stall control principles. Note increased starting torque for pitch controlled turbine at λ=0

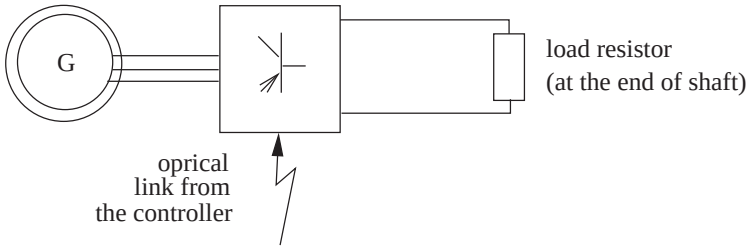

Figure 3.4: Schematics of Optislip drive

tional speed constant or even brake it and thereby to cause the operating point on the $c_P(\lambda)$ -curve to move to smaller tip speed ratio values. In this method, the blades are stalled to separate flow from the upper (suction) side of the profile. Stall is a very complex phenomenon, because separated flow is turbulent and because in wind turbines air also flows along the blade and attaches flow again, making it hard to model the process precisely. The blades are often designed so that their root section stalls first and the separation bubble then moves back and forth along the blade: it moves back as the blade encounters slow wind speeds in the downright position and forth as the blade is upright in strong upper winds. Some hysteresis, called "stall delay," also occurs to postpone entry into stall even if the angle of attack were wide enough [18].

Stall is also a problem in terms of control. As we see later, the turbine becomes unstable as the operating point moves to the left of the peak on the $c_T(\lambda)$-curve. That is, the feedback from changing from rotational speed to aerodynamic torque has a positive sign. As the speed and the tip speed ratio increase, aerodynamic torque increases, thus increasing the speed even

further. Countering this problem is discussed more thoroughly in Chapter 5.

To create specified stall behavior, the blade designer uses several methods. As the twist angle differs from the optimal, especially at its tip and root (i.e. geometrical twisting), this and different profiles can be used along the blade (i.e. aerodynamical twisting of the blade). Using thicker profiles at the root is necessitated also by structural demands. That this is mentioned in a thesis on wind turbine control demonstrates the fine borderline between blade design and wind turbine control. Because of modern computer programs, wing characteristics can be largely simulated in advance, though we are still unable to fully compute three dimensional stall behavior.

In real grid conditions, fluorescent lamp ballasts, induction motors, and transformers act as an inductive load. A self-commutated bridge such as the one used in this application can compensate this load by producing capacitive reactive power. Hence the need for additional capacitor batteries is eliminated.

3.2 Commercial variable speed drives

The variable speed drive was first realized by the Austrian Villas in its 600 kW model. The plant also had pitch control, but because of its expensive power electronics, among other problems, it was not a commercial success. Also the German Enercon introduced a variable speed turbine with a rating of 80 kW and fixed blades as well as the first commercial direct-drive for medium-size wind turbines in 1993 for a 500 kW WT with pitch control. Direct drive generators are also used by Lagerwey of the Netherlands [49], Jeumont of France [51], and ABB of Sweden [5] in its later cancelled Windformer project. The last two use permanent magnet generators, Windformer even a medium-voltage generator.

Only recently have other manufacturers begun employing variable speed drives. The most common solution among them is the Scherbius cascade, which consists of an asynchronous generator with a wound rotor. The stator windings of the asynchronous generator (ASG) are here also connected directly to the grid, but the rotor windings are connected to the grid via slip rings and a frequency converter (FC). The generator's rotational speed can be on both sides of the synchronous speed $n_{sync} = f/p$, where f is the frequency and p the number of pole pairs. At oversynchronous speeds, i.e., over 1500 rpm for the four-pole generator in a 50 Hz grid, the power lost as heat in the squirrel-cage bars of the generator is fed in the wound rotor generator into the grid. At subsynchronous speeds, power is fed from the grid into the rotor winding and again back into the grid via the stator [9], [28]. Initially, the

Scherbius cascade was used widely in large, multi-megawatt pump storages and in high power applications, like wind power, where torque is proportional to rotational speed squared. A part of the power (25–30%) flows via the FC, resulting in a cheaper FC. A disadvantage here is that the slip ring brushes wear out and require biannual service, a fact which must be considered on sites of difficult access, like offshore wind farms.

A compromise between the direct drive and the geared drive with a high gear ratio, e.g. 1:100, is the Multibrid concept [6], which makes use of a medium speed (100-200 rpm) generator and a moderate ratio gearbox 1:10. Thus problems with temperature, durability of high speed gears and generators, and excessive size and weight of direct-drive generators are obviated. From the electrical point of view, the Multibrid concept resembles the direct drive generator, a synchronous generator connected to the grid via an FC. The Finnish WinWind wind turbine makes use of a permanent magnet generator (PMG) [52].

The gearless PMG vs. the geared asynchronous generator is discussed in [78]. Both wind turbine drives were discussed in [75] along with various ways to realize variable speed drive.

3.3 Variable speed control trajectory used

In this section, an optimal control trajectory is presented on the aerodynamic torque -rotational speed -plane, $T_a - \omega_t$. The efficiency of the turbine is maximized in the wind speed region of the highest energy content. Rotational speed and (aerodynamical) power input are restricted to the nominal to prevent overspeeding and -loading. Finally, an important feature is pointed out: power input can be limited below nominal with variable speed control only in case the grid or battery cannot receive full output.

The power coefficient c_P is multiplied by Eq. (2.1) to yield the power produced by the turbine:

$$P_{turb} = \frac{\rho}{2}\pi R^2 v_t^3 c_P(v_t, \omega_t, \beta). \tag{3.2}$$

The aerodynamic torque acting on turbine blades is obtained respectively:

$$T_a = \frac{\rho}{2}\pi R^3 v_t^2 c_T(v_t, \omega_t, \beta). \tag{3.3}$$

As we can see, turbine power and speed depend on

- the air density, ρ. The colder the air, the denser it is. At high altitudes, the air is thinner.

- the swept area of the turbine πR^2 (perpendicular to wind). If the turbine is turned away from wind, the swept area becomes smaller
- wind speed, v_t
- the power coefficient, c_P, and the torque coefficient, c_T, which depend on the pitch angle, β and the relation between blade tip speed and wind speed. In this thesis the pitch angle is not controlled.

The only way to control the wind turbine is therefore to regulate the relationship between rotational speed and wind speed. It is done by controlling the generator torque and further the rotational speed.

3.3.1 Below maximum power

Let us take as an example a turbine designed for a small wind turbine. At a wind speed of 9 m/s, we obtain the curves for power and torque coefficient in Fig. 3.5. The figure shows that the three-bladed turbine has its best power coefficient when the tip speed ratio is between four and five, i.e., when the blade tip advances four and a half times as fast as the air. These curves hold for any wind speed, because we ignore distortions such as those caused by the Reynolds number.

We may now choose any point $(\lambda_0, c_{P,0})$ on the $c_P(\lambda)$-curve we want to track. To maximise energy production in the below rated power region we choose the point where the power coefficient is at its maximum $(\lambda_{opt}, c_{P,opt})$. Combining the formulae (3.2) and (3.3), we obtain a relation between aerodynamic torque and rotational speed,

$$T_a = \frac{\rho}{2}\pi R^5 c_{P,0}\frac{1}{\lambda_0^3}\omega_t^2 = k_T\omega_t^2, \tag{3.4}$$

where k_T is obtained by:

$$k_T = \frac{\rho}{2}\pi R^5 c_{P,0}\frac{1}{\lambda_0^3}, \tag{3.5}$$

which realizes the optimum operating point regardless of wind speeds. This control path formulation on the $T_a - \omega_t$-plane was introduced in [10].

As we can see, aerodynamic torque is in a quadratic relation to rotational speed as some point $(\lambda_0, c_{P,0})$ has been chosen. When we measure the rotational speed ω_t and estimate the aerodynamic torque $\hat{T}_a$, we can find out if the wind turbine works at the desired operating point or not (See Section 4.4).

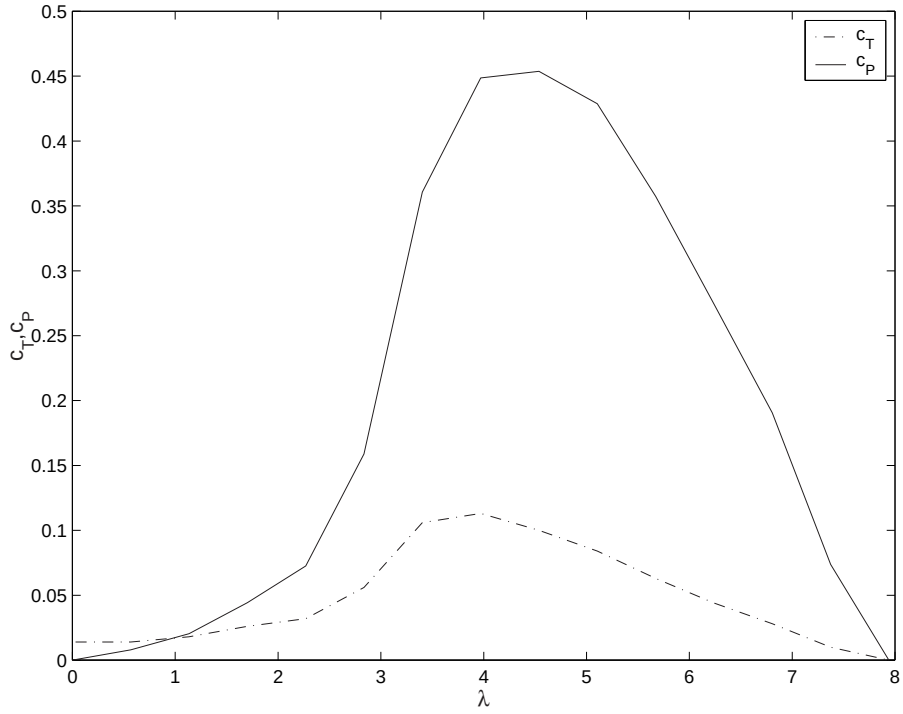

Figure 3.5: Power (c_P) and torque coefficient (c_T) versus tip speed ratio (λ) for a small wind turbine

To realize the control, it is more convenient to give equation (3.4) in the form [76]:

$$\omega_{opt} = \omega_{ref} = \sqrt{\frac{\hat{T}_a}{k_T}} = k_W \sqrt{\hat{T}_a}, \tag{3.6}$$

where

$$k_\omega = \frac{1}{\sqrt{k_T}} = \sqrt{\frac{2\lambda_0^3}{\rho \pi R^5 c_{P,0}}}. \tag{3.7}$$

The optimal (reference) rotational speed is obtained from estimated aerodynamic torque by Eq. (3.6). Note that wind speed is not mentioned in this equation.

3.3.2 Above maximum power

As wind speed exceeds the rated value, the power extracted from the wind must be restricted. Solutions to implement this restriction were not available in the literature. Generally, the maximum allowed aerodynamic power is the

rated power $P_{max} = P_n$. If the electric grid or battery cannot receive even the rated power, the maximum power may be much lower.

The maximum aerodynamic power extracted by turbine equals

$$P_{max} = k_T \omega_{max}^3 \tag{3.8}$$

vice versa

$$\omega_{max} = \sqrt[3]{\frac{P_{max}}{k_T}}. \tag{3.9}$$

We can now calculate the maximum torque T_{max} at each maximum power P_{max}

$$T_{max} = k_T \omega_{max}^2 \tag{3.10}$$

and as ω_{max} is replaced by (3.9), the maximum torque is given by

$$T_{max} = k_T (\frac{P_{max}}{k_T})^{\frac{2}{3}} = ... = k_T^{\frac{1}{3}} P_{max}^{\frac{2}{3}}. \tag{3.11}$$

Formula (3.11) has a $\frac{2}{3}$- exponent, which for an 8-bit microcontroller is very time-consuming to calculate. However, in Fig. 3.6 we can see that the dependency is nearly linear and that we can therefore use a linear approximation. The constant $k_T^{\frac{1}{3}}$ can be calculated in advance and stored in the memory of the controller.

When aerodynamic torque exceeds the calculated T_{max} value, power is limited and unoptimised, and the rotational speed reference is given by

$$\omega_{ref} = \frac{P_{max}}{\hat{T}_a}. \tag{3.12}$$

3.3.3 Intermediate power

In the intermediate region, rotational speed is kept constant,

$$\omega_{ref} = \omega_c, T_1 < T_a < T_2, \tag{3.13}$$

where

$$T_1 = \frac{\omega_c^2}{k_\omega^2} \tag{3.14}$$

and

$$T_2 = \frac{P_n}{\omega_c} \tag{3.15}$$

A simpler alternative to the former is to calculate the speed reference with below/above-rated equations and then limit this speed reference to ω_c, as is done with small wind turbines.

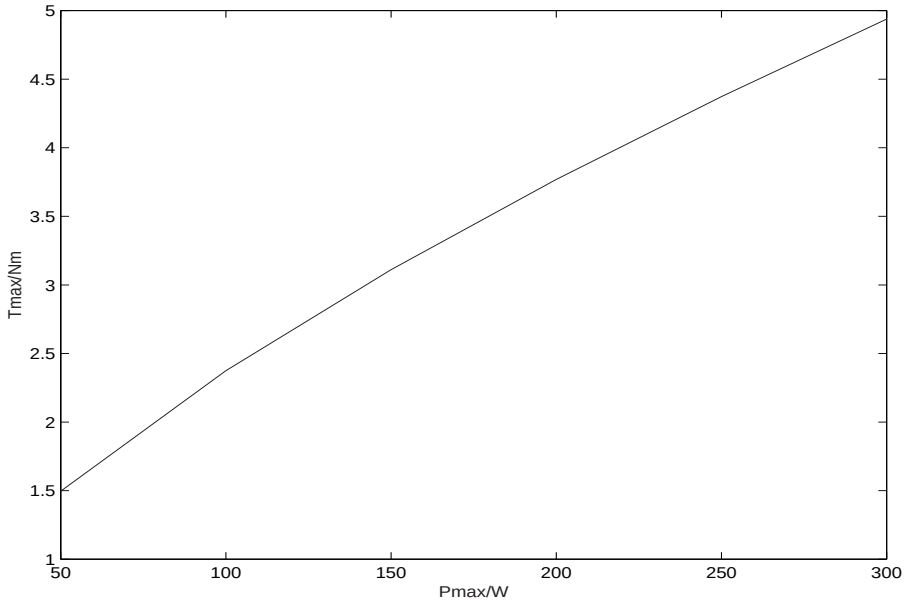

Figure 3.6: T_{max} as function of P_{max}

3.3.4 Summary of speed reference formation

The rectified (permanent magnet) generator voltage exceeds the battery voltage at ω_{min} equal to ca. 150 rpm. Therefore, ω_{ref} must not be lower than ω_{min}. Indirectly, this restricts the power from below. There is a minimum for power taken from the turbine. In a formula:

$$\omega_{ref} = \begin{cases} k_\omega \sqrt{\hat{T}_a}, & \hat{T}_a \leq T_1 \\ \omega_c, & \hat{T}_a > T_1. \end{cases} \tag{3.16}$$

However, if $\hat{T}_a > T_{max}$

$$\omega_{ref} = \frac{P_{max}}{\hat{T}_a}. \tag{3.17}$$

To summarise the result, the rotational speed reference is formed as in Fig. 3.7 from the estimated aerodynamic torque $\hat{T}_a$. Equation (3.11) holds well throughout the speed region and defines the switch point between the optimizing and limiting control path on the $\hat{T}_a - \omega_{ref}$ -plane. In addition, the reference is restricted to the maximum ω_c and minimum ω_{min}.

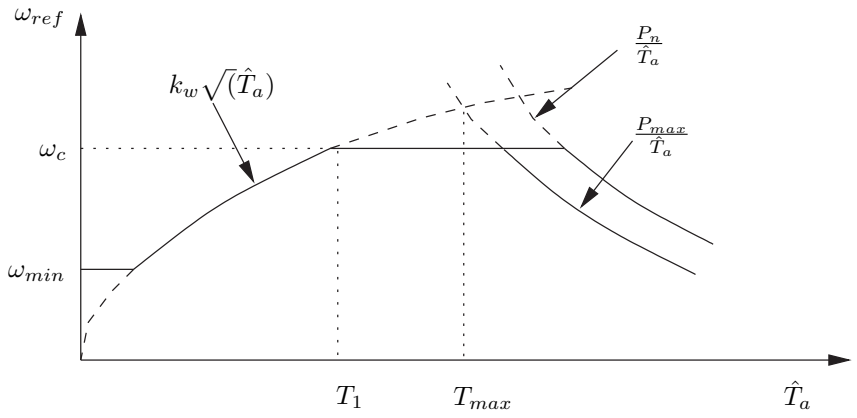

Figure 3.7: Rotational speed reference formulation from estimated aerodynamic torque

3.4 Variable speed control configurations

The variable speed, fixed pitch (VSFP) turbine has inspired only a few research papers. Connor and Leithead and their group at the University of Strathclyde have published papers on the controller design of this concept and used mainly classical controllers, excluding PI-controllers with and without gain scheduling [13], [14], [16], [36].

Ekelund and Novak [54] compared the PI, $\omega^2 - T$, $\omega - \sqrt{T}$ control paths with LQG control. They linearized their plant around certain operating points and then simulated it. They also employed other methods, using the Kalman filter for state estimation, but had problems with gain scheduling and transition from one operating point to another.

Ernst-Cathor [21] examined an adaptive scheme for wind turbine control. The control parameter k_T in the formula $T_{ref} = k_T\omega_t^2$ is constantly varied and changed to find a better optimum. At above rated wind speeds, the power is limited by blade pitch control. Convergence is here rather slow and takes 30-60 minutes to find an optimum, the slowness being caused by a cautious adaptation algorithm, as only slow adaptation is required in normal operation.

Mercer and Bossanyi [44] compared variable speed-variable pitch (VSVP) and variable speed-fixed pitch (VSFP, the concentration of this thesis) machines quantitatively. Their results indicated no major difference in the price of the electricity produced, when other compared components such as the blades, nacelle, and tower of the different wind power plants were equal.

The possibility to control both rotational speed and pitch angle allows the

most degrees of freedom for wind power plant control. Furthermore, we can control the generator voltage, if we use an electrically excited synchronous generator, which allows four times slower pitch control than the FSVP, as the turbine temporarily speeds up during gusts, absorbing their energy. In addition, the output of the VSVP can be more easily limited [81] to suit the carrying capacity of the grid or night time noise regulation.

Controlling a VSVP plant is a multiple input-multiple output (MIMO) problem. We have now two control inputs available. According to Leithead [36], the configuration may be simplified with a diagonal controller, i.e., the generator's rotational speed is controlled by fast power electronics and its power by adjusting the pitch angle. With the state feedback controller, the problem is reduced to two single, parallel input-single output (SISO) problems with the diagonal gain matrix K_k. In the below-rated wind speed region, the pitch angle is kept constant, and the plant becomes again, like the FPVS machine, an SISO problem. Also Cardenas-Dobson deals with variable speed-variable pitch machines with aerodynamic torque estimation [11], [12].

Chapter 4

Modelling the wind power drive

4.1 Modeling the wind field on the rotor plane

The models of wind speed variation are based on white noise, filtered by various wind models that act as band-pass filters within a range of $2 \cdot 10^{-5} - 10$ Hz to cause a notch in the power spectrum. The state-space model of the wind speed v_t may be given by a first order model,

$$\dot{v}_{t,lin} = -\frac{1}{T_v} v_{t,lin} + m(t), \tag{4.1}$$

where m is white Gaussian noise. Eq. (4.1) has a spectral density function of

$$\Phi_v(f) = \frac{K_v}{1 + (T_v \cdot \omega)^2}, \tag{4.2}$$

where K_v and T_v are constants. Among other wind turbulence models, the most commonly used is the von Karman spectrum [38]:

$$\Phi_v(f) = \frac{K_v}{1 + (T_v \cdot \omega)^{\frac{5}{6}}}. \tag{4.3}$$

The time constant T_v and the turbulence intensity $\sigma_{v,lin}$ are obtained by empirical formulae:

$$T_v = \frac{10.5z}{v_0} \tag{4.4}$$

$$\sigma_{v,lin} = \frac{\sigma_v}{v_0} = \frac{0.88}{ln(\frac{z}{z_0})}, \tag{4.5}$$

where z is the height above the terrain, v_0 median wind speed at point of reference and z_0 the roughness length.

4.1.1 Spatial filtering

Typically, only one point is inspected in real wind speed measurements or in artificial wind data from given equations. Measurements are taken with a cup anemometer, which has its own time constant of 0.3–0.4 s. This equals a 2–2.7 m distance constant; e.g., the typical Vaisala standard anemometer. When we use a cup anemometer, we should correct the sampled data by filtering it with the inverse transfer function of the anemometer (the first order model will suffice). When we use a sonar or heated wire anemometer, this factor vanishes because of the meter's negligible time constant.

However, this measured or artificial one point wind data is averaged over the swept area of the rotor, the rotor area itself acting as a low-pass filter with a transfer function [40] of

$$G_{ra}(s) = \frac{\sqrt{2} + \beta_s s}{(\sqrt{2} + \beta_s s\sqrt{a})(1 + \frac{\beta_s}{\sqrt{a}} s)}. \tag{4.6}$$

In Eq. (4.6) the nominal parameters have empirical values of $a = 0.55$ and $\beta_s = \phi_d R/v_t$. The decay factor over the disc, ϕ_d, is chosen empirically as 1.3. The filter, with its DC-gain clearly one, reduces power at higher frequencies.

This effect is seen in comparing measured one point wind speed data with filtered data (Fig. 4.1). The spatial filter improves the accuracy of the modelled spectrum. Low-pass filtering and the averaging effect of the turbine plate transfer power from higher to lower frequencies, see Fig. 4.2.

4.1.2 Tower shadow

When the blades pass the tower, variation occurs in shaft torque with a frequency of $z_b\omega_t$, where z_b is the number of blades. The tower shadow effect is most marked in down-wind turbines, where the turbine is located leeward of the tower, and the effect is stronger with wind turbines with a tubular than with a truss tower. In the common up-wind turbines, the tower shadow has some effect on the power spectra of the wind in the turbine disk.

4.1.3 Induction lag

According to [82], induction lag occurs when the blades react to a change in wind speed and hence to a changing angle of attack. This over/undershot can be modelled as a lag filter as follows:

$$I_l(s) = \frac{a_i s + \frac{1}{\tau_i}}{s + \frac{1}{\tau_i}} = \frac{a_i s + b_c}{s + b_c}, \tag{4.7}$$

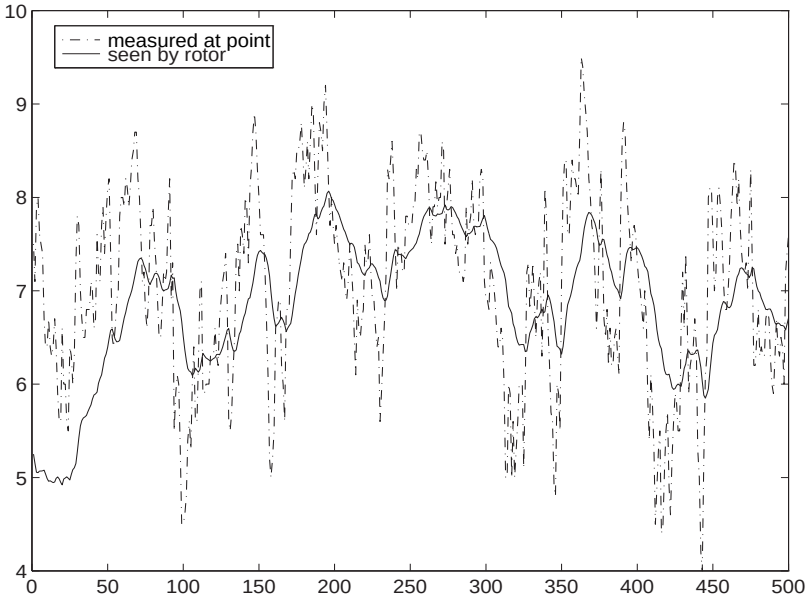

Figure 4.1: Wind speed measured at one point and filtered with a spatial filter

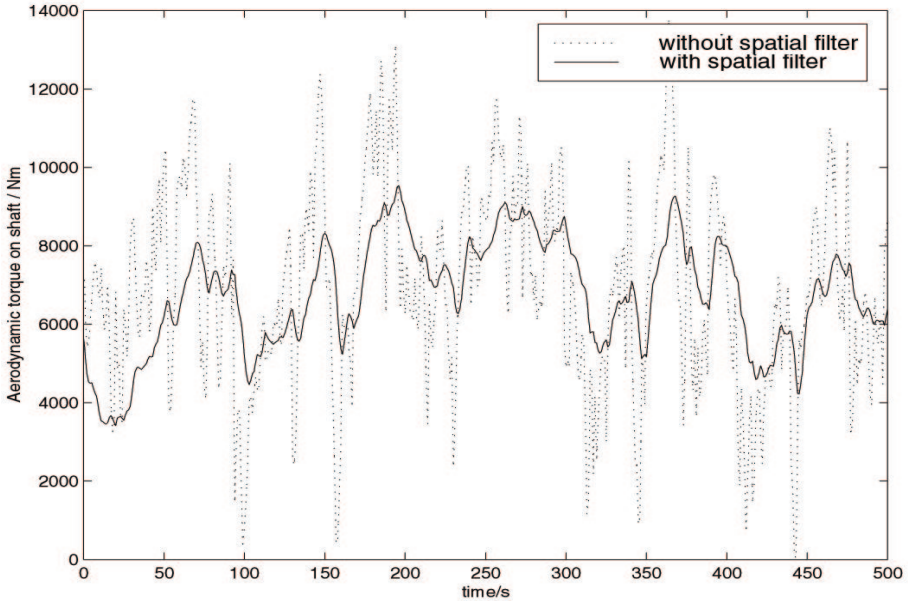

Figure 4.2: Low speed shaft torque before and after inclusion of a spatial filter

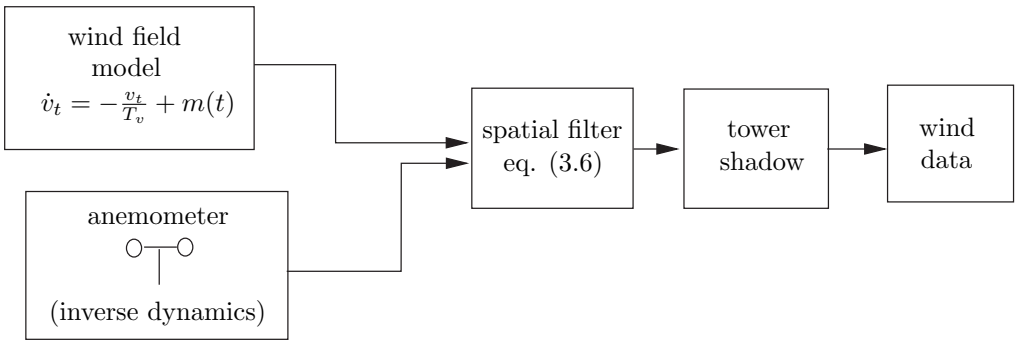

Figure 4.3: Process for obtaining valid data for simulations

where $a_i > 1$ and amplifies certain mid-range frequencies. In [82], the wind speed was about 12 m/s, the time constant, τ_i, nine seconds, and the empirical parameter identification for a_i measured 1.37. Hence the procedure to obtain valid wind simulation data may be characterised as in Fig. 4.3. Wind speed is measured as filtered with an appropriate inverse transfer function of the anemometer, and the data is then passed through the transfer functions of a spatial filter and thereafter used as input in wind turbine simulation. The induction lag is to be added after the $c_T(\lambda)$ - function of the turbine.

The process to obtain wind data for simulations is described in Fig. 4.3. In the literature, many authors have not applied spatial sampling and are therefore providing misleading simulation results with a too rapidly altering wind speed. [63] provides a more extensive study of wind models.

However, the following assumptions have been made in wind field modeling:

- no wind shear, either vertical or horizontal is taken into account
- the height gradient of wind speed, i.e., the Prandt logarithmic law model in ($\frac{\overline{v}_t(z)}{v(H)} = \frac{\ln(z/z_0)}{\ln(H/z_0}$,) where $\overline{v}_t(z)$ is the mean wind speed at height z compared to a reference height H in terrain with a surface roughness of z_0. [23]
- variations in the horizontal direction of wind speed are not considered; perfect tracking in the yaw direction is assumed; in practise, this is not possible and causes 1-2% energy loss and additional stress on components

4.2 Modelling the turbine

In modelling the drive train, emphasis should be placed on the turbine itself, as the other drive train components can be analyzed with common methods. Aerodynamic torque is non-linear with respect to the tip speed ratio and the pitch angle. This relation, $c_T(v_t, \omega_t, \beta)$, may be modeled with splines [74], with look-up tables [15], as in this thesis, or by fitting in the exponential function

$$c_T(\lambda) = C_1 \lambda e^{-C_2 \lambda}, \tag{4.8}$$

where C_1 and C_2 are positive, real numbers.

To analyze the turbine with linear methods, the non-linear torque function in (4.8) may be linearized by taking into account only the first terms of the Taylor series. Aerodynamic torque is then expressed as

$$T_a = \frac{\rho}{2} \pi R^3 v_t^2 c_T(v_t, \omega_t, \beta). \tag{4.9}$$

The $c_T(\lambda)$ -curve is now linearized with respect to wind speed, rotational speed, and pitch angle (in the pitch controlled turbine) at a given operating point (O.P.) $x_0 = [\omega_{t,0}\ v_{t,0}\ \beta_0]^T$,

$$\Delta T_a = \theta \Delta v_t + \gamma \Delta \omega_t + \kappa \Delta \beta, \tag{4.10}$$

where

$$\theta = \frac{\partial T_a}{\partial v_t} \mid_{O.P.} = C_0 \omega_t (2 c_{T,0} - \lambda_0 \frac{\partial c_T}{\partial v_t} \mid_{O.P.}) \tag{4.11}$$

$$\gamma = \frac{\partial T_a}{\partial \omega_t} \mid_{O.P.} = C_0 R \omega_0 \frac{\partial c_T}{\partial \omega_t} \mid_{O.P.}) \tag{4.12}$$

$$\kappa = \frac{\partial T_a}{\partial \beta} \mid_{O.P.} = C_0 \frac{\partial c_T}{\partial \beta} \mid_{O.P.} \tag{4.13}$$

$$C_0 = \frac{\rho}{2} \pi R^3 \tag{4.14}$$

$$\lambda_0 = \frac{\omega_{t,0} R}{v_{t,0}}, \tag{4.15}$$

where $\partial c_T / \partial i$ is a partial derivate of the torque coefficient.

In a linearized situation, the derivative of aerodynamic torque multiplied by wind speed may be regarded as an external disturbance. Linearized (with respect to an operating point) wind speed may be modelled by employing, e.g., the von Karman or von Kaiman wind speed models.

If we employ the pitch angle β as a means of control, we should then calculate also the linearized coefficient, κ. Before the pitch angle, we should

model the dynamics of the pitch actuator with a wind turbine model, e.g., with first order dynamics. The derivatives of $\partial T_a/\partial\beta$ are obtained from blade design calculations or by identification with real-life tests. Since this thesis deals with the stall-regulated configuration, no further attention is paid to pitch input.

4.3 Modeling the drive train

Novak et al. [54] modeled the wind power drive with a two-mass model using a slowly rotating part. The turbine and its hub were modeled as one and the first part, the generator and gears as the other mass. These were scaled appropriately with the gear ratio to the low speed side. The drive shaft was considered a flexible joint between the two masses. However, during identification, Novak noticed that the outer parts of the turbine blades formed the first mass and the hub and the generator a second mass because of the flexibility of the blades compared to a stiffer drive shaft [20]. A two-mass model is also discussed in [54], whereas a very comprehensive modeling was performed in [8].

In this thesis and for simplicity, the wind power drive is modeled as one mass to highlight the drive's most difficult features. However, we must consider the resonance frequencies that arise especially in large wind power plants. The following assumptions were made in modeling the turbine:

- no interaction between the drive train and tower dynamics; i.e. no tower dynamics are taken into account (no tower)
- no gravitational forces, acting on a single blade and causing periodic excitation, are considered
- the blades and the whole rotor are considered as a single, lumped mass

A one-mass model for wind turbine drive is as follows:

$$\dot{\omega}_t = \frac{T_a - T_g - B_t\omega_t}{J_t}, \tag{4.16}$$

where $\dot{\omega}_t$ is the angular acceleration of the turbine, T_g the generator torque, B_t the damping of bearings and seals, and J_t the combined inertia of generator and turbine (dominating).

The derivative of aerodynamic torque with respect to the rotational speed, γ, may be considered as aerodynamic damping. In laminar flow, its sign is clearly negative, and it thus stabilizes the transfer function from electrical torque to rotational speed. In the stall region, aerodynamic damping becomes positive, resulting in an unstable transfer function.

4.4 Kalman filter and wind turbine model

Aerodynamic torque is modeled as the first order Markov process, i.e., as inertia driven by noise

$$\dot{T}_a = -\frac{1}{T_L}T_a + \xi, \tag{4.17}$$

where T_L is the time constant of aerodynamic torque and ξ normally distributed noise whose variance is R_1.

Thus, a state-space model is obtained

$$\begin{aligned} \dot{x} &= Ax + Bu + v_1 && (4.18)\\ y &= Cx + v_2, && (4.19) \end{aligned}$$

where x is a state vector, A the system matrix, B the input matrix, u controlled inputs, C the measurement matrix, and v_1, v_2 system and measurement errors, respectively. When (4.16) and (4.17) are merged, we have

$$\begin{aligned} \begin{bmatrix} \dot{\omega}_t \\ \dot{T}_a \end{bmatrix} &= \begin{bmatrix} -\frac{B_t}{J_t} & \frac{1}{J_t} \\ 0 & -\frac{1}{T_L} \end{bmatrix} \begin{bmatrix} \omega_t \\ T_a \end{bmatrix} + \begin{bmatrix} \frac{1}{J_t} \\ 0 \end{bmatrix} T_g + \begin{bmatrix} 0 \\ \xi \end{bmatrix} && (4.20)\\ y &= \begin{bmatrix} 1 & 0 \end{bmatrix} \begin{bmatrix} \omega_t \\ T_a \end{bmatrix} + \eta, && (4.21) \end{aligned}$$

where η is normally distributed measurement noise with a variance of R_2 and y is the measurement. Here we measure only the rotational speed of the turbine, ω_t.

However, for simulation purposes, the continuous-time model is discretized with the first order approximation

$$e^{Ah} \sim I + Ah, B = hB, \tag{4.22}$$

where h is the sample time used in the calculations. Hence the discrete system matrices will be:

$$A_f = \begin{bmatrix} 1 - h\frac{B_t}{J_t} & \frac{h}{J_t} \\ 0 & 1 - \frac{h}{T_L} \end{bmatrix}, B_f = \begin{bmatrix} \frac{h}{J_t} \\ 0 \end{bmatrix}, C_f = \begin{bmatrix} 1 & 0 \end{bmatrix}, D_f = [0], \tag{4.23}$$

whereupon the discrete system will be:

$$\begin{aligned} \hat{x}_{k+1} &= A_f\hat{x}_k + B_f u_k + w_k = \\ \begin{bmatrix} \hat{\omega}_{t,k+1} \\ \hat{T}_{a,k+1} \end{bmatrix} &= \begin{bmatrix} 1 - h\frac{B_t}{J_t} & \frac{h}{J_t} \\ 0 & 1 - \frac{h}{T_L} \end{bmatrix} \begin{bmatrix} \hat{\omega}_{t,k} \\ \hat{T}_{a,k} \end{bmatrix} - \begin{bmatrix} \frac{h}{J_t} \\ 0 \end{bmatrix} T_{g,k} + \begin{bmatrix} 0 \\ \xi \end{bmatrix} && (4.24)\\ y_k &= C_f\hat{x}_k + D_f u_k + v_k = \\ \omega_{t,k} &= \begin{bmatrix} 1 & 0 \end{bmatrix} \begin{bmatrix} \hat{\omega}_{t,k} \\ \hat{T}_{a,k} \end{bmatrix} + \eta. && (4.25) \end{aligned}$$

The Kalman filter [32] works with the following equation:

$$\hat{x}(k+1 \mid k) = A_f \hat{x}(k \mid k-1) + B_f u(k) + K_f(k)[y(k) - C_f \hat{x}(k \mid k-1)]. \quad (4.26)$$

The factor $K_f(k)$ is the Kalman gain matrix, and it is updated as

$$K_f(k) = A_f P_x(k) C_f^T [C_f P_x(k) C_f^T + R_2(k)]^{-1}. \quad (4.27)$$

The time-variant covariance matrix can be computed recursively,

$$\begin{aligned} P_x(k+1) &= \\ A_f P_x(k) A_f^T &- A_f P_x(k) C_f^T [C_f P_x(k) C_f^T + R_2]^{-1} C_f P_x(k) A_f^T + R_1(k), \end{aligned} \quad (4.28)$$

where R_1 and R_2 are state model error and measurement error covariance matrices, respectively. Because R_1 and R_2 are considered time-invariant, the Kalman gain matrix, K_f, can be computed here in advance. Formula (4.26) can be modified to make it somewhat easier for computation. The state estimate at the moment k can be updated with

$$\begin{aligned} \hat{x}(k+1 \mid k) &= \begin{bmatrix} \hat{\omega}_t(k+1 \mid k) \\ \hat{T}_a(k+1 \mid k) \end{bmatrix} = \\ (A_f - K_f(k) C_f) \hat{x}(k \mid k-1) &+ B_f T_g(k) + K_f(k) \omega_t(k). \end{aligned} \quad (4.29)$$

Also: Now that we have the previous estimate $\hat{x}(k \mid k-1)$, i.e., the previously calculated $\hat{\omega}_t$ and $\hat{T}_a$ and the measured generator torque (T_g; calculated from the torque-producing component of the generator current), and the rotational speed of the turbine ω_t, we can obtain the best possible estimate of the next moment: the estimate of the rotational speed $\hat{\omega}_t$ and that of the aerodynamic torque $\hat{T}_a$. The Kalman filter acts as a model-based method and calculates an optimal estimate of the state vector. Results are then compared with measurements from a real-time model. A more extensive presentation of the Kalman filter appears e.g., in [27].

These models were simulated extensively and have been described earlier in [75] for a two-mass drive, i.e., the inertias of turbine and generator were connected with a flexible shaft. These simulations were repeated later in the test bench setting of a large wind energy converter. However, because of numerical problems, the simulations vibrated considerably and are therefore not repeated here.

Chapter 5

Controller design and simulations

5.1 General

A classical controller design is based on a cascaded three-loop control structure used in electrical power drives. In Fig. 5.1, the innermost loop is an armature current controller, controlling the power electronics so that the current tracks the reference value without exceeding preset values. The next loop constitutes a speed controller, which ascertains the error between the speed reference and actual speed and then gives a current reference. The position controller lies in the outermost loop and follows the position reference. The further inside the controller, the faster it is bound to be. Driving torque, explained in more detail in reference [39], is seen as a disturbance and is placed between the current controller and the drive.

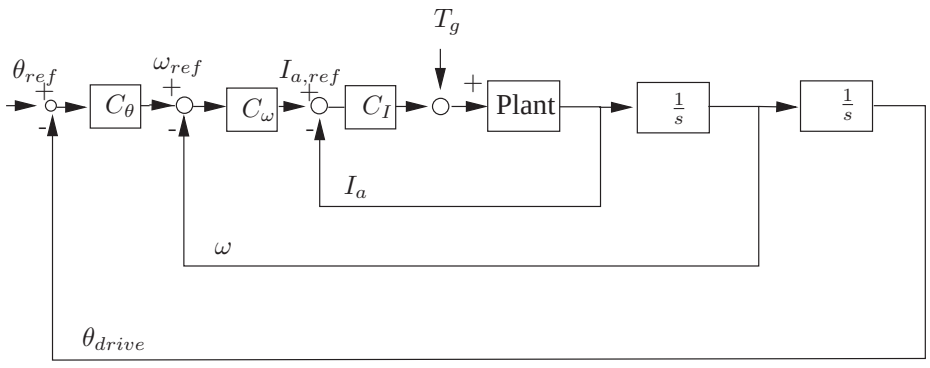

Figure 5.1: General electrical drive control configuration

In our case, the outermost position controller was not needed at all, for the speed reference was obtained with a reference model. Estimated aerodynamic torque and rotational speed were used to determine the most favorable control strategy and accordingly to give a reference to the speed controller (the control strategy was explained in Section 3.3). The innermost loop, which is the armature current control, was omitted in this study as the time constants of the power electronics were much smaller than the mechanical ones.

The most important task of the speed controller is to stabilize the plant at all operating points. The biggest problem with stall regulated wind power plants is the aerodynamic damping γ, which causes the plant's transfer function to have a real, negative, or positive pole. This means that the wind turbine is an uncertain system, because of the variation in γ. Furthermore, the wind turbine becomes unstable in a stall, as the pole formed by γ in $(\gamma - B_t)/J_t$ moves to the right half plane as γ becomes positive. The term B_t may be ignored in this stability consideration, since $|\gamma| >> |B_t|$. In terms of classical control, this means that the speed controller should be designed to set all the poles onto the left half-plane, a task which is not so difficult if a laminar flow occurs at all operating points. Then $\gamma < 0$, and the plant is stable and only uncertain. The pitch-controlled plant (excluding those applying the assisted stall control principle) is stable in the above-rated region, or any plant in the below-rated region that falls in this category.

We can ensure the stability of the plant at all operating points in two ways. One is to use robust control with constant parameters. According to this method, the inner loop stabilizes the plant in all conditions by state-variable feedback, i.e., by multiplying the states and feeding them back as input into the plant. This results in a proportional or proportional-derivate (P/PD) type controller. In the proportional type controller, rotational speed is measured, multiplied by the proportional control constant K_p, and fed back as generator torque input. To ensure the stability of the plant, the condition $K_p > \max(\gamma)$ should be fulfilled to bring the pole $(\gamma - B_t)/(J_t)$ back to the left half-plane. Such proportional (P) control satisfies the stability requirement but may perform sluggishly, especially in the above-rated power region. The performance depends greatly on the linearizing time frame of rotational speed. In this control configuration, a steady-state torque value should be added to the torque given by the controller. To obtain the linearized value, the steady-state rotational speed value should also be subtracted from the instantaneous value,

$$T_g = K_p \Delta\omega_t + T_{g,0}. \tag{5.1}$$

An asynchronous generator already meets this requirement, since it has a

very steep $\omega_g - T_g$ -curve: The nominal torque is produced at a slip of 3-4%, and it is capable of three times the nominal torque before stalling.

We cannot consider here a single, purely integral type controller because the sign of the system gain can be positive or negative, and such a controller could therefore not stabilize the plant under all operating conditions. If we use two linear controllers with an integral part (PI/PID), we may encounter windup difficulties as one controller is always switched off. Furthermore, in this application, the integral controller's task to drive the steady-state error to zero is not important because the set point is constantly changing due to changing wind speed; an integrating controller is thus of little practical value. Moreover, the turbine itself acts as an integrator.

5.2 Two switched PI-controllers

Since the turbine is stable at below-rated wind speeds and unstable at above-rated wind speeds, the first idea is to use very crude scheduling with one controller setup for each area, as is done with several overlapping LQG controllers [7]. These were simulated with a 100 kW model and reported in [80] and compared with initial fuzzy control. However, switching as the turbine was verging on instability caused overshooting and vibration in output. In simulation, this controller structure ensured plant stability with sufficient results.

5.3 Aerodynamic torque feedforward

The basic idea about the feedforward used here comes indirectly from [20]. The feedforward of aerodynamic torque is also incorporated in Model Based Predictive control, applied in [63].

Aerodynamic torque is added to the state vector of the wind power plant, i.e. $x = [\omega_t \quad T_a]^T$. In this approach, an estimate of this extended state is fed back:

$$\begin{aligned} \begin{bmatrix} \dot{\omega}_t \\ \dot{T}_a \end{bmatrix} &= \begin{bmatrix} -\frac{B_t}{J_t} & \frac{1}{J_t} \\ 0 & -\frac{1}{T_L} \end{bmatrix} \begin{bmatrix} \omega_t \\ T_a \end{bmatrix} \\ &+ \begin{bmatrix} \frac{1}{J_t} \\ 0 \end{bmatrix} T_g + \begin{bmatrix} 0 \\ \xi \end{bmatrix} \qquad (5.2) \\ y &= \begin{bmatrix} 1 & 0 \end{bmatrix} \begin{bmatrix} \omega_t \\ T_a \end{bmatrix} + \begin{bmatrix} \eta \end{bmatrix} \qquad (5.3) \end{aligned}$$

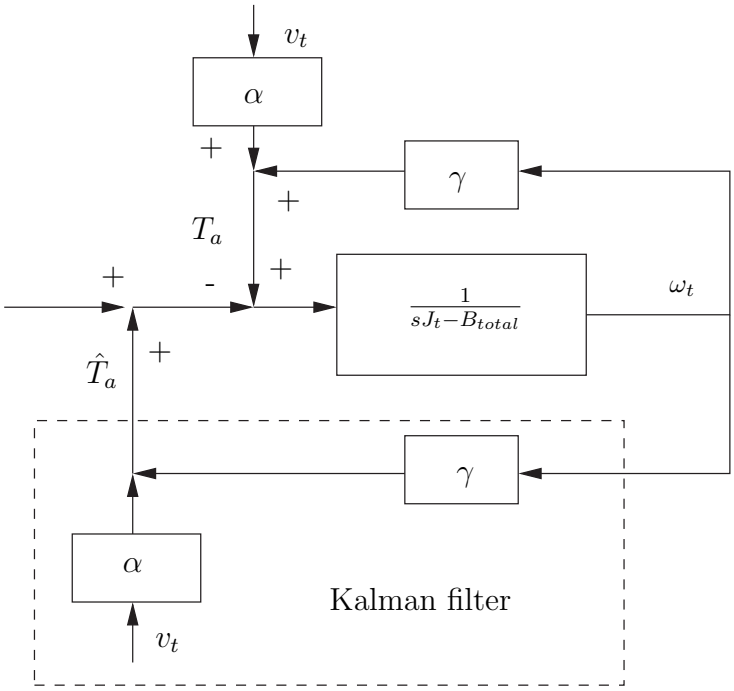

Figure 5.2: Effective pole cancellation in Eq. (5.6)

$$T_g = \begin{bmatrix} K_p & 1 \end{bmatrix} \begin{bmatrix} \hat{\omega}_t \\ \hat{T}_a \end{bmatrix} - K_p \omega_{ref}. \tag{5.4}$$

Since

$$T_a = \gamma \omega_t + \theta v_t, \tag{5.5}$$

and we set $B_{total} = B_t + B_g$ for the one-mass model, the pole of the plant in the closed loop becomes

$$p_0 = \frac{-\gamma - B_{total}}{J_t} + \frac{\gamma + K_p}{J_t} = \frac{-\gamma - B_{total}}{J_t} + \frac{\gamma + K_p}{J_t} = \frac{K_p - B_{total}}{J_t}. \tag{5.6}$$

This idea is shown schematically in Figs. 5.2 and 5.3. The position controller in Fig. 5.1 is replaced by maximum power control, as explained in Section 3.3. This control strategy was introduced in [75] and [79].

The pole $(\gamma - B_{total})/J_t$ is in effect cancelled and placed in a new position $(K_p - B_{total})/J_t$. The value of the feedback component $K_p(\hat{\omega}_t - \omega_{ref})$ should be within 10-30% of nominal torque, depending on the compromise made between rapidity of response and minimization of torque and current peaks.

An added benefit is the absence of linearization, since estimated aerodynamic torque is fed directly back into the plant and the difference between

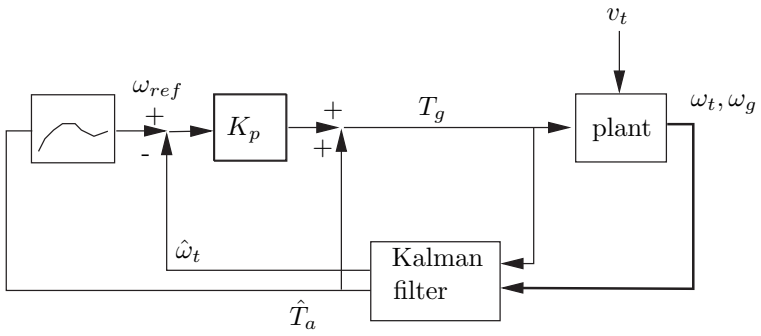

Figure 5.3: Controller structure used

the reference and actual rotational speed is used. Hence we have no problems with real time linearization.

A similar control structure is used in robotics, e.g., in [84] to compensate for unmodeled dynamics, load variations, and the ageing of the equipment. This control structure was also used in [48] but only with an ordinary torque observer and in the above-rated wind speed region.

Because aerodynamic torque is fed back into the plant as a part of the control input, the aerodynamic damping term vanishes. Furthermore, the disturbance of wind speed variation is simultaneously compensated. As aerodynamic torque cannot be measured, it can be estimated by the Kalman filter as shown in Section 4.4. Linearisation causes problems because aerodynamic torque is a non-linear function of rotational and wind speed. While the controller can be considered very fast, aerodynamic torque can be regarded as a state, driven by white noise, and therefore estimable with the Kalman filter. Consequently, we can place the dominant pole freely in any suitable place.

One problem in the two-mass system is the effect shaft flexibility has on performance. Another is that unless the pole is not properly cancelled, we may have a non-minimum phase system, and the plant is in the above-rated power region. This scheme is, in practice, a step toward a LQG filter, in which we can clearly see a continuously changing feedback factor of rotational speed via an indirect estimation of aerodynamic torque and, therefore, an indirect estimation of γ. This corresponds to changing the feedback constant, as in LQG control.

The other alternative is to have multiple controllers, at least one LQ/LQG controller for each region [7] or multiple control criteria for one controller, as in [20]. The difficulty of this approach is scheduling between the different controllers. In [20], the controller itself remained the same all the time, but the weighting parameters Q_1 and Q_2 for state and for control were scheduled

according to the operating point.

5.4 Fuzzy control

The concept of fuzzy sets was introduced by Lukasiewitz et. al. in the 19th century. Fuzziness means here that something can simultaneously belong to several sets and can, therefore, be simultaneously empty or full, true or false. The difference between two states is only a matter of a different combination of degrees of membership in several sets. Lotfi Zadeh [83] combined these sets with 'if-then'-reasoning and thus turned them into fuzzy logic.

It is worthwhile to apply fuzzy logic to control, if a given process is strongly non-linear or its mathematical model is difficult to develop, or the model is complex or time-variant. Fuzzy logic mimics human reasoning and experience and thus enables automatization of tasks, such as driving a car and speech and pattern recognition, which require heavy computing if linear methods are used. Alternatively, fuzzy logic relies on non-exact values and parallel computing to perform its tasks. Furthermore, fuzzy operations can be realized directly on a hardware level, thus reducing computing time. With fuzzy logic one can directly realize a nonlinear controller with restrictions, such as saturation of actuators, which are incorporated and calculable in the controller design.

On the other hand, to reach an optimal solution, fuzzy logic requires careful planning. Because it is not based on mathematical models, transparency and familiar concepts such as stability and phase margin are lost. In many published papers, PI-control is replaced by fuzzy PI-control, which is a non-linear controller and the easiest application of fuzzy logic to control but does not necessarily fully exploit the possibilities of fuzzy control. One should not consider fuzzy logic without first studying the possibilities of conventional control methods. For example, adaptive control may often be applied equally well to a given problem. Often a fuzzy controller owes its superiority only to the number of parameters in the designed controller. A fuzzy controller with fifty parameters performs better than a linear, two-parameter PI-controller. However, one can ask whether the same result could be achieved with a ten-parameter linear controller. Moreover, fuzzy logic is used all too often to control the innermost, fastest control loops, whereas it is actually better suited for something higher up in the control hierarchy.

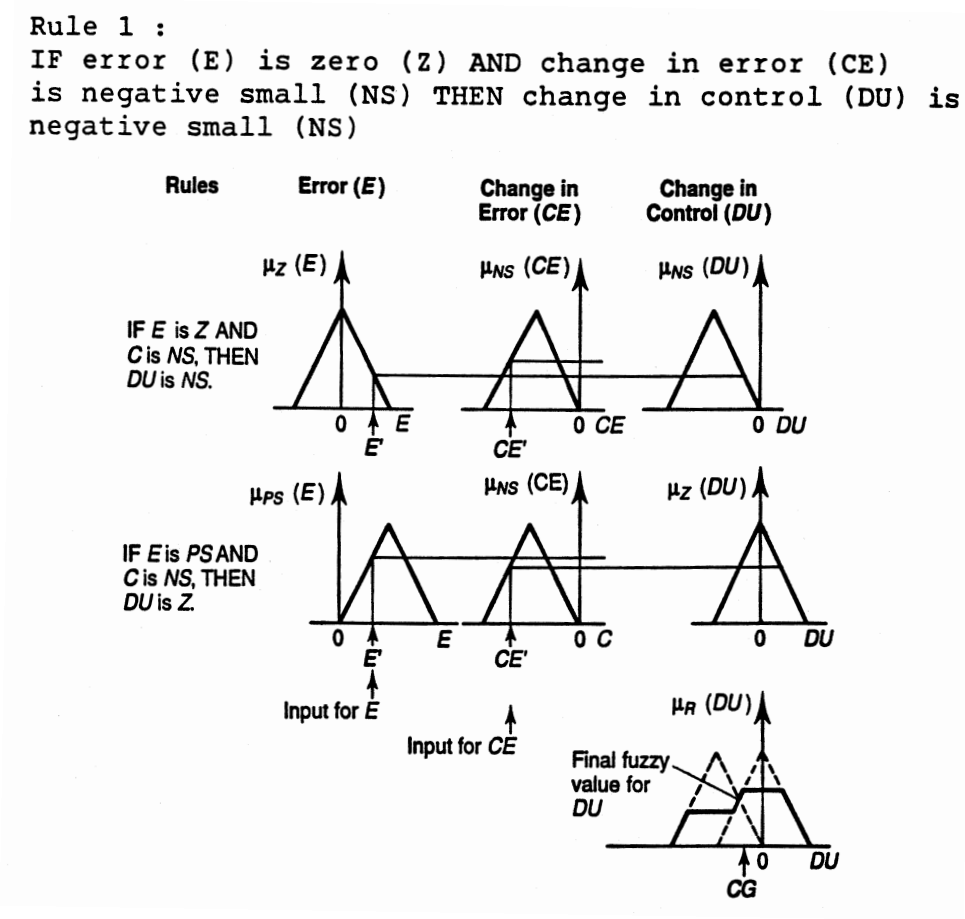

Figure 5.4: Fuzzy reasoning process

5.5 General fuzzy control design process

Fuzzy control is based on the idea that the input space is converted by fuzzy sets into verbal concepts such as "small," "medium," "big," whereby fuzzy reasoning is carried out and the results are defuzzified into real numbers. The result is not obtained by one rule only but by a multiple of these rules.

The design process of a fuzzy controller can be characterized as follows [9].

1. Analyze whether a fuzzy controller is needed or whether classical control would be more appropriate.

2. Get all the information available on the process concerned, its function and principles from a system designer, if possible.

3. If a mathematical model of the system exists, simulate it with a classical controller and analyze the performance.

4. Define the points where fuzzy control is needed.

5. Define the input and output variables of the fuzzy controller.

   With statistical methods, one can determine the effect of a given input on the outputs and thus focus on the most important rules.

6. Define the range of the former.

7. Define the fuzzy set and the respective membership functions. More rules should be available for the most influential variables.

   The density of the membership functions should be high in the regions where the plant is very nonlinear. In general, a triangle function is used in the input space, where the sum of the input functions is one, i.e., a neighbouring function ends where another function has a peak value of 1. It is useful to design input rules so that they saturate, i.e., have a value of 1 outside the predetermined region. Thus control still works even though the input exceeds the predetermined range. Output membership functions are usually singletons, i.e., columns which are computationally the lightest.

8. Define the rule base.

   Here we use verbal definitions such as "IF x is SMALL AND y is MEDIUM, THEN output z is ZERO." At this point, we should define the decision method for comparing the rules, among which MIN-MAX-reasoning is the most common. The rule base can be composed into a rule table with abbreviations such as Negative (N), Positive (P) , big (B), and small (S). The design programs of fuzzy controllers usually allow the controller to be viewed in a graphical form, as a so-called decision surface, whose shape can be modified by changing the rules or methods of reasoning. The surface should be smooth without slopes, bumps, or roughness, and its edges should saturate to a given value. Highly nonlinear areas are modeled with densely placed fuzzy rules.

   In the design process, the controller is viewed as a black box with known inputs and outputs. The process may sometimes, as with a pulp digester or a cement kiln, be so complicated that no mathematical model exists for it. The rules can also be found out in verbal form by interviewing an experienced operator. The result of the process is a

rule table (Table 5.1), shown graphically as a reasoning surface in Fig. 5.5.

9. Define the scaling factors for inputs.

10. If a mathematical model exists, simulate the system with a fuzzy controller at various operating points. If no model exists, design a fuzzy controller in line with a classical controller and tune it with a real process under the supervision of a human operator.

    If the result does not amount to what is expected, rules or outputs should be changed. The more nonlinear, unstable, and uncertain (badly modeled) a given process is, the more difficult it is to tune the rule base. Tuning may be accomplished through self-tuning or a learning neuro-fuzzy controller. As in optimal control, the controller is optimized by different criteria for error, control, and elapsed time. For example, with MATLAB one can study the behavior of a controller on reasoning surfaces by tracing process inputs on the surface. The process should make use of the whole surface but not exit it.

11. Implement the fuzzy controller in real-time form and further enhance its performance. Like other controllers, the fuzzy controller is realized with a microcontroller or a control computer. But we should also solve the problems with a real solution, noise, delays, and unmodeled dynamics.

5.6 Fuzzy controller design

This section expounds on the main points of the fuzzy controller used in the study and designed by Pasi Ridanpää (for more details, see [60], [62]). The model is similar to those used in classical wind turbine control.

Fuzzy logic has been applied to regulate the variable speed of wind power plants in the below-rated power region [31], [67], where the system is stable and where a relatively simple maximum power point tracking controller is sufficient. What has been unavailable though is a fuzzy control that would cover all the operating points of the variable speed wind power plant, both stall and pitch regulated. Responding to this lack, this thesis examines the whole operating region of the stall regulated wind power plant.

Most crucial in the design of a fuzzy controller is to find the right inputs and outputs. A fuzzy controller does not receive all the inputs directly as measurements but is accompanied by an estimator and a pre-calculator, the most important of which is the one that estimates the aerodynamic torque $\hat{T}_a$ and which operates according to Eq. (3.4). Unlike the classical controller,

which uses speed reference, our controller makes use of torque reference. This is the same formula turned the other way around.

5.7 Fuzzy controller in the above rated region

Aerodynamic torque can be obtained indirectly by an observer whose inputs are the generator torque, T_g, and the rotational speed of the generator, ω_g, or by the measured rotational speed of the turbine, ω_t. Generator torque is linearly dependent on the current in the DC-circuit of the CS-inverter, as commutation is not taken into account, whereas rotational speed is linearly dependent on the source voltage of the generator.

When these are known, and to estimate the aerodynamic torque, $\hat{T}_a$, we should decide whether to use only the generator torque, T_g , or to include also the effect of drive train inertia. The optimal operating point is tracked purely with the generator torque T_g and the friction losses $(B_g + B_t)\omega_t$. The error [14]

$$e_1 = T_g + B_{total}\omega_t - T_{ref} \tag{5.7}$$

is minimized. Aerodynamic torque is estimated as

$$\hat{T}_a = T_g + B_{total}\omega_t + J_{total}\frac{\partial \omega_t}{\partial t}. \tag{5.8}$$

In the above equation, the total inertia of the drive train $J_{total} = J_t + J_g$ and the total viscous damping coefficient, B_{total}, i.e., the friction losses of the drive train, $B_{total}\omega_t = (B_t + B_g)\omega_t$, are taken into account. In this case, the error e_2 to be minimized is

$$e_2 = T_g + B_{total}\omega_t + J_{total}\frac{\partial \omega_t}{\partial t} - T_{ref}. \tag{5.9}$$

These two options can be combined with a weighting variable ε. Typically, ε has a value ranging between 0 and 1, and it gives the combined torque error of the controller, i.e.,

$$e = (1-\varepsilon)e_1 + e_2 = T_g + B_{total}\omega_t - T_{ref} + \varepsilon J_{total}\frac{\partial \omega_t}{\partial t}. \tag{5.10}$$

With (5.7)-(5.10), we can calculate the current operating point on the $\omega - T$-plane and the reference point $(\omega_{opt}, T_{a,opt})$, and thus also the distance between these points. In the below-rated power region, we optimize energy production and track the $T_a = k_T\omega^2$ -curve. In the above-rated power region, we should track $T_a = \frac{P_2}{\omega_t} - k_2$, where P_2 and k_2 are well chosen constants.

The fuzzy controller receives six inputs:

1. The estimated aerodynamic torque, $\hat{T}_a$
2. Change in the estimated aerodynamic torque, $\Delta\hat{T}_a$
3. The rotational speed of the generator, ω_g
4. Change in the rotational speed of the generator , $\Delta\omega_g$
5. Error in the below-rated torque reference, e_{be}, given by (5.9)
6. Error in the above-rated torque reference, e_{ab}, given by (5.9)

The inputs are obtained through the aerodynamic torque observer, as described in Eq. (4.16). One output of the fuzzy controller is change in generator torque, and that makes it an integral type controller.

The fuzzy controller decides whether the operating point $(\hat{T}_a, \omega_t)$ should track the below- or the above-rated curve. Generator torque is then increased or decreased according to the error sign in the set point and the change sign in rotational speed, indicating the operating point's departure from or approach to the set curve. Furthermore, a single step rule is there to increase generator torque if the turbine speed reaches the nominal speed. This rule also facilitates transfer from the below- to the above-rated curve with increasing wind speed and vice versa. The problem of wind turbine control is that the chosen control method affects the next reference value. The wind turbine controller controls simultaneously the turbine so that it reaches the given reference value, which the controller provides. The fuzzy controller calculates this reference value from the turbine speed with the formula $T_{be,ref} = k_T\omega_t^2$ or $T_{ab,ref} = P_n/\omega_t$. A complete list of the membership rules is given in [75].

The fuzzy controller is superior to the conventional controller at the point when operation is transformed from the below- to the above-rated region or vice versa. At this point, a switch occurs between two conventional controllers or an abrupt change in the reference value given by the outer control loop. The fuzzy controller is inherently better able to manage this variation since the transition between the two states happens in it more smoothly than in the classical controller we studied.

Table 5.1: Fuzzy rule table of a controller with $\Delta\omega_t$ and e_1 to ΔT_g when T_a is small

$e_1 \setminus \Delta\omega$	nb	nm	ns	zero	ps	pm	pb
nb	nm	nm	nm	ns	nss	ze	ze
ns	nm	ns	ns	nss	ze	ze	pss
ze	nss	nss	ze	ze	ze	pss	pss
ps	nss	ze	ze	pss	ps	ps	pm
pb	ze	ze	pss	ps	pm	pm	pm

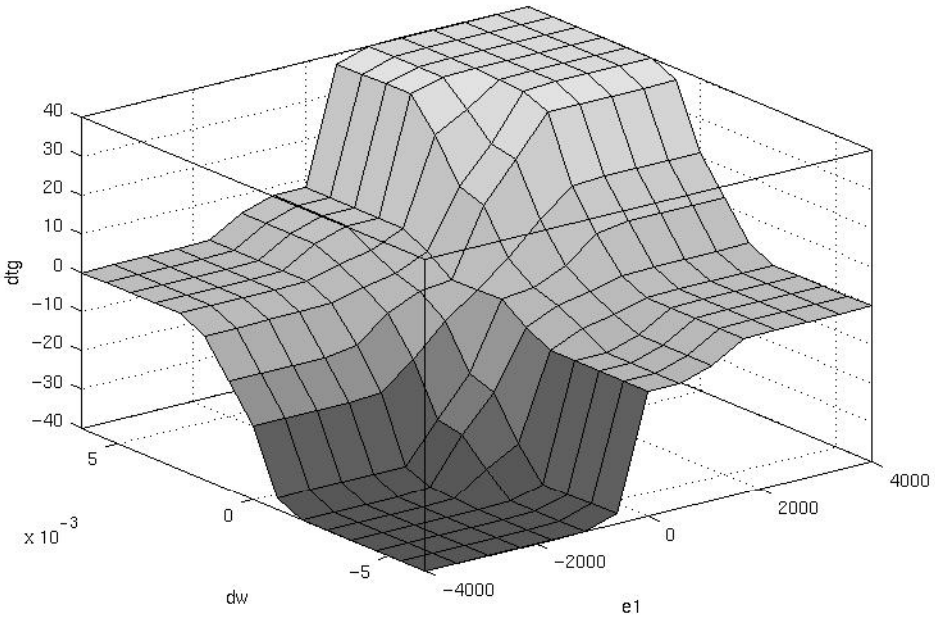

Figure 5.5: Reasoning surface based on the rule table in Table 5.1

Chapter 6

Testing the large wind power drive

6.1 Description of test plant

This chapter describes the configuration of a large-scale wind power test bench. The overall configuration of the test arrangements is shown in Fig. 6.1, and each main component is treated in its own subsection.

6.1.1 Turbine

The turbine was replaced by an ordinary asynchronous motor (250 kW, 992 rpm), and the force was transferred by a chain belt drive with a transmission ratio of 5:1. The chain was kept tight by an additional wheel (Fig. 6.2), though despite tightening, the chain belt tended to hop now and then. Additional struts were used to strengthen the somewhat weak mechanical structure of the generator.

The asynchronous motor was driven by a frequency converter (ACS 600), manufactured by ABB [2] and exploiting the so-called Direct Torque Control algorithm (DTC), which controls motor torque directly by comparing observed air gap torque with reference torque. The reference torque comprised aerodynamic torque plus the simulated inertia of the turbine, which corresponded to the power plant's drive train torque.

Aerodynamic torque was created by simulation. Recorded wind data with a sample time of 1 Hz was filtered to correspond to the wind field of a 20 meter diameter turbine (see Section 4.1). A wind speed and an estimated rotational speed were fed into formula (3.3) (other parameter values used are listed in Appendix A). Measured wind data was then fed into the computer model, which simulated the $c_T(\lambda)$-curve of a real turbine.

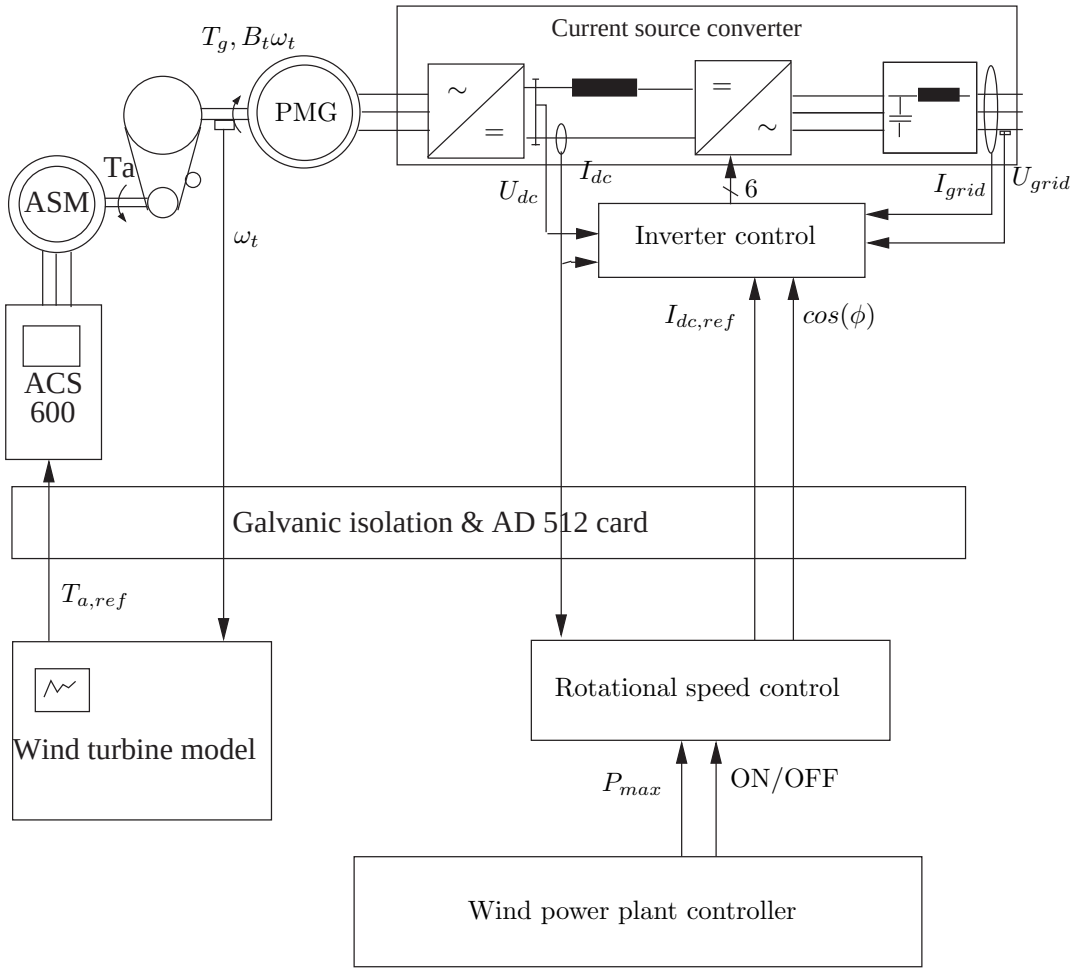

Figure 6.1: Control bench schematics for a large wind power drive

An induction lag was included [40], and the resulting aerodynamic torque was filtered with the transfer function

$$G = \frac{J_{t,sim}s + B_{t,sim}}{J_{drive}s + B_{drive}}, \tag{6.1}$$

where $J_{t,sim}$ and $B_{t,sim}$ are simulated total drive inertia and damping, respectively, and J_{drive} and B_{drive} are the real values of the test bench.

Transfer function (6.1) was used for the reference signals of both aerodynamic ($T_{a,ref}$; to the ACS 600) and generator ($T_{g,ref}$; PMG FC) torque. The turbine model was thus run on the same computer as the controller, but separately, and the models shared only the estimated rotational speed (see Fig. 6.2).

The aerodynamic torque reference was transmitted as a standard 4-20 mA current signal to the ACS 600. Because of very high measured nominal torque (16 kNm), no torque transducer was placed between motor and generator. The asynchronous motor torque was considered to match the aerodynamic torque reference. The chain transmission ratio (5:1) was taken into account in forming the torque reference.

6.1.2 Generator

The wind power generator we tested was a gearless, 100 kW permanent magnet generator (PMG) with an outer diameter of 2.5 m (Fig. 6.2). The technical details of the test arrangement are listed in Appendix A. The generator was designed and built at TUT with its large parts manufactured by subcontractors. In topology, the generator was an axial flux generator, as in Fig. 1.1, consisting of a toroidally wound stator ring, surrounded on both sides by rotor iron rings. Permanent magnets were attached to the rotor rings and magnetized so that the magnetic flux was parallel to the generator shaft in the air gap [69], [70] and [71].

Because of its high torque rating, the generator had a low rotational speed. The large diameter was also economical, as costs were minimized over 20 years of operation and included only a few expensive magnets and low current densities (see [56]). The small force in the air gap had to be compensated for by a wide generator radius to yield the required torque. In other words, with the same rating and rotational speed, the generator could have been only 1 m in diameter, but very expensive. Energy losses were also kept low by low current densities. The low rotational speed and magnetic flux densities were achieved by using six parallel three-phase systems in the generator.

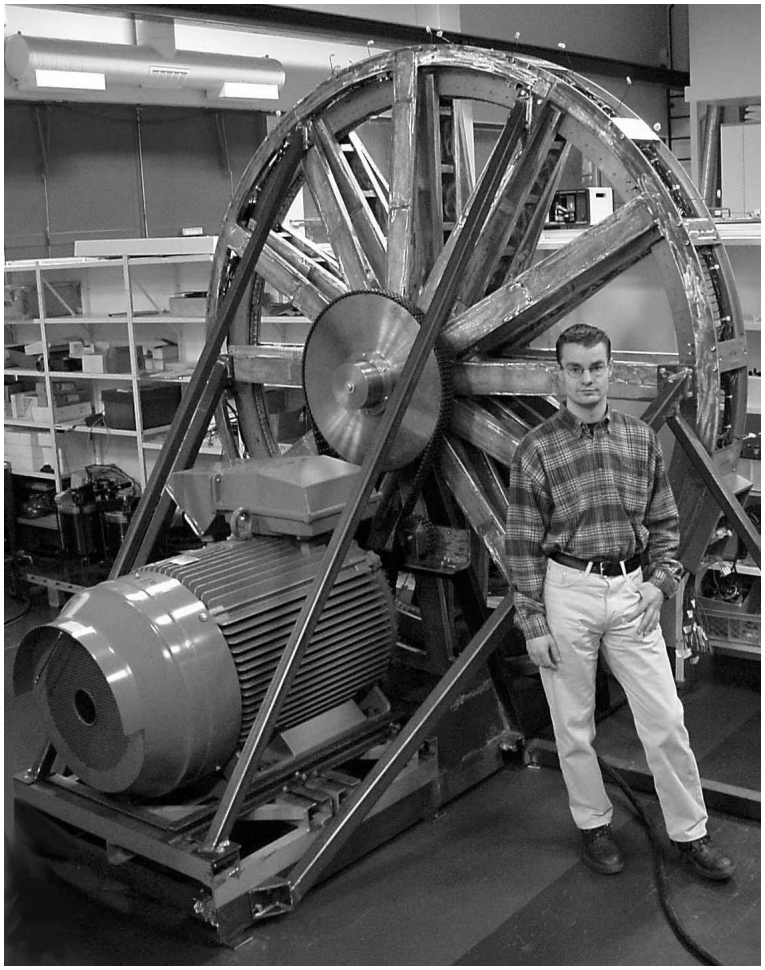

Figure 6.2: Test arrangement of a large wind power drive. Permanent magnet generator on right, asynchronous motor down left, chain belt transmission in middle

In the tests, the generator produced a trapezoidal voltage wave form because of its concentrated winding. It was also tested at constant rotational speeds without a control system [33], [34], [58].

6.1.3 Current-source frequency controller

As the permanent magnet generator is electrically a synchronous machine, it cannot be connected to the grid directly because it may fall out of synchronism during gusts [75].

The power was fed into the grid via a frequency converter (Fig. 6.3), which used a 60 kW current-source converter with a 100 kW peak power rating. A three-phase electrical current was rectified by a six-pulse diode bridge, and the direct current was fed into a large inductor coil connected on the other side to a grid bridge consisting of six insulated gate bipolar transistors (IGBT). By controlling the IGBTs, we could regulate the power fed into the grid. Also the reactive power could be controlled. In this case, the power factor was set to 1, i.e., the drive did not produce inductive or capacitive reactive power in the tests. Details of the frequency converter (FC) and the static test bench runs appear in [34], [46] and [59].

Generator torque was controlled by the DC-circuit current. The actual generator torque was considered linearly dependent on reference to the DC-current in the speed control loop due to the fast current control loop. The time constant of the current control was 3-4 milliseconds, but the time constant of the speed control was several seconds. The current reference was brought to the frequency converter via a 0-5 V voltage signal, galvanically separated from the computer.

6.2 Test bench parameters

The damping of the drive, B_{drive}, was identified by rotating an unloaded drive at various speeds. Because of the wide diameter, the inertia of the drive, J_{drive}, was dominated by the permanent magnet generator and tested by rotating the drive at nominal speed with no load and then cutting off the driving torque. The time for the drive to stop was measured. The inertia can be obtained as described in [39].

Fig. 6.1 shows the schematics of the large test bench with the current source converter in the top middle and right. The only control input into the wind power drive was generator torque. In this configuration, generator torque was controlled by the current in the DC circuit of the frequency converter. The controller of the inverter bridge controlled the DC current, I_{dc},

Figure 6.3: Current source converter, the leftmost

and the power factor of the power fed into the grid, $\cos(\phi)$. This is why we needed to measure the grid voltage and the current, U_{grid}, I_{grid}.

The speed controller received the rotational speed, ω_g, and the DC current, included a Kalman filter according to Eqs. (4.24) and (4.24), and determined the optimal speed reference described in section 3.3. The plant controller, which was higher in the control hierarchy, switched the plant on and off. The system also had an option to regulate the maximum output power, P_{max}. Furthermore, the wind turbine model received rotational speed measurements and calculated the corresponding aerodynamic torque of the modeled turbine.

Because of the reactance of the generator windings, generator torque is a linear function of the DC current only at small current values. The gap between the torque reference and the actual generator torque was observed with a special configuration of the Kalman filter, in which this gap was assumed to be a disturbance and the Kalman filter was fed only in this case with aerodynamic torque, i.e., the torque reference to the ACS 600. The generator torque reference was proportional to rotational speed squared to simulate real operating conditions.

As T_g was not equal to $T_{g,ref}$, an additional torque component, called $T_{g,gap}$, was included in Eq. (4.16). This component can be considered an extra rotating torque on the shaft,

$$T_a = J_t \frac{\partial \omega_t}{\partial t} + T_{g,gap} - T_g - B_t \omega_t. \tag{6.2}$$

A parallel Kalman filter was deployed with its state consisting of the estimated rotational speed and the additional torque component $[\hat{\omega}_t \quad \hat{T}_{g,gap}]^T$. The inputs to the parallel filter were the true aerodynamic torque (T_a, here: torque reference to the ACS 600) and the generator torque (T_g, here: current reference to the current source frequency converter). For the parallel Kalman filter, the matrices will be (compare with Eq. (4.24)):

$$\begin{aligned}
\hat{x}_{k+1} &= A_{gap}\hat{x}_k + B_{gap}u_k + w_k \\
&= \begin{bmatrix} \hat{\omega}_{t,k+1} \\ \hat{T}_{g,gap,k+1} \end{bmatrix} \\
&= \begin{bmatrix} 1 - h\frac{B_t}{J_t} & \frac{h}{J_t} \\ 0 & 1 - \frac{h}{T_L} \end{bmatrix} \begin{bmatrix} \hat{\omega}_{t,k} \\ \hat{T}_{g,gap,k} \end{bmatrix} \\
&- \begin{bmatrix} \frac{h}{J_t} & -\frac{h}{J_t} \\ 0 & 0 \end{bmatrix} \begin{bmatrix} \hat{T}_a \\ \hat{T}_g \end{bmatrix} \begin{bmatrix} 0 \\ \xi \end{bmatrix} \\
y_k &= C_{gap}\hat{x}_k + v_k = \omega_{t,k}
\end{aligned} \tag{6.3}$$

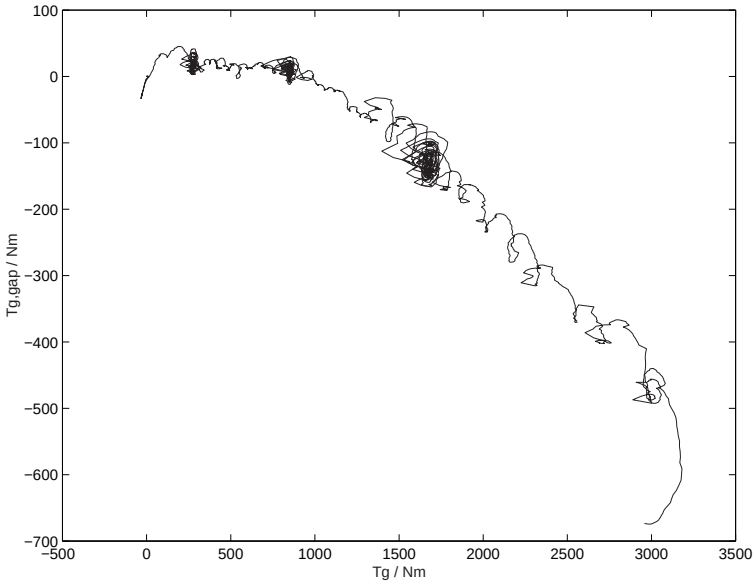

Figure 6.4: Gap between generator torque reference and actual generator torque ($T_{g,gap}$)

$$= \begin{bmatrix} 1 & 0 \end{bmatrix} \begin{bmatrix} \hat{\omega}_{t,k} \\ \hat{T}_{g,gap} \end{bmatrix} + \eta. \tag{6.4}$$

A second degree spline curve fit was plotted for the torque gap as a function of the generator torque reference, and the gap was then added to the generator torque reference

$$T_{g,ref} = T_{g,ref} + T_{gap}(T_{g,ref}). \tag{6.5}$$

On a successive observation of reference vs. actual generator torque, no significant gap appeared anymore. The generated power was fed into the grid. It should be pointed out that this commutation problem, i.e., a nonlinear relation between rectified generator current and generator torque arises only with a machine-commutated bridge and a medium or a high generator rating. In later tests in the Laboratory of Power Electronics, a self-commutated generator bridge with power transistors matched the generator torque with a reference. Commutation was not a problem with the small 300 W generator, as shown in Section 7.2.

Speed was measured with a Tekel TK 510 pulse encoder [68], mounted on the other end of the PMG shaft. Its 500 pulses/revolution were far too few for good control purposes. The sample time of the control was 0.1 s, and

the generator rotated at 30 rpm. One sample time can consist of 9-11 pulses resulting in a 10% measurement error, as shown in Fig. 6.7. However, from the viewpoint of Kalman filtering, this made the task more challenging. The pulses were converted to a 0-5 V DC voltage signal [57], corresponding to speeds of 0-60 rpm.

The ACS 600 and the current source frequency converter were controlled by a 200 MHz Pentium PC, running Windows 95, Matlab 5.2 [42] and Simulink 2.0 [43]. As MATLAB itself is not a real-time program, we used an additional Real Time Toolbox [29] and an 8-bit Analog/Digital/Analog card AD 512 by Humusoft ([30]). The PC was protected against electricity shocks by galvanic isolation, and the analog signals were separated with Siemens IL300 components [66].

The main Simulink block diagram, controlling the motor that simulated a wind turbine and the current rectifier that drove the generator are shown in Fig. 6.5. Note that the rotational speed, ω_t, obtained with the Kalman filter was fed into the wind turbine model and resulted in less noise in aerodynamic torque. On the left, we have a separate block to simulate the higher inertia of the turbine and in the middle a large block to communicate with the measurement card. This block scales the input and output signals.

The Simulink block for the Kalman filter and the rotational speed control loop is shown in Fig. 6.6. Note how the friction torque, $B_t\omega_t$, is removed here from the generator torque. The removal was later eliminated as performance improved. In the small generator, this configuration was used for relatively high damping, especially in the test bench. The Kalman filter is expressed in Eq. (4.26), and its inputs are measured rotational speed and generator torque.

6.3 Test runs

The nominal rotational speed of the generator is 60 rpm, but for safety reasons it was run at a maximum of 30 rpm, which restricted its maximum power to 12.5 kW. Steady-state tests with constant speed and power are described in [34].

6.3.1 Below-rated control

The most time consuming task during the tests was the manual tuning of the measurement covariance matrix R_2, which had to be done because the estimates of aerodynamic torque and rotational speed were too erroneous. If the values of R_2 are too small, estimates vibrate about the true value; if they

are too large, the filter becomes sluggish and estimates fall behind the true values.

Furthermore, ω_{ref} had to be filtered with a low-pass filter with a transfer function of $0.8/(s+0.8)$ to assure that the time constants of the outer control loop were greater by a decade than those in the inner loop. The drive vibrated but as $J_{t,sim}$ was increased to $28 \cdot 10^3$ kg/m^2, the vibration ceased, and the drive behaved well.

Because of the power electronics, all measurement signals had much noise (see Fig. 6.7). In future tests, a better noise-prone bus such as CAN,IEEExxx should be used to minimize the impact of an electromagnetically noisy environment.

6.3.2 Above-rated control

In the initial test runs, the rotational speed hunted about the reference in the above-rated power region, which was the most difficult to control. As the plant entered the above-rated region for the first time, a strong, increasing vibration was observed with a cycle time of 12.5 s when the rotational speed exceeded the speed limit. The hunting was corrected when the term $(B_t + B_g)\hat{\omega}_t$ was removed from Eq. (6.2). In effect, such hunting causes more damping in the wind drive due to a steeply rising generator torque at increasing speeds. Furthermore, the hunting corrugated when $J_{t,sim}$ was increased to correspond to a real 100 kW turbine (Fig. 6.8). In the upper figure, all variables are normalized; e.g., the rotational speed is divided by ω_n.

6.3.3 Fuzzy control

Because the fuzzy control was thought to be immune to measurement noise, an aerodynamic torque observer was used, based on differentiation of speed, as in Eq. (4.16). This resulted in a very high variation in generator torque, because the controller had been tuned to a lower level of measurement noise. Subsequently, we deployed also a Kalman filter as in classical control to estimate aerodynamic torque and rotational speed. This combination produced a very good response from the control, despite some vibration around the nominal power (Fig. 6.9).

6.4 Discussion

The main requirement for a control system and stability was fulfilled throughout the operating envelope, and the wind power drive behaved reasonably well

in the below- and above-rated wind speed regions. Because of the inherent instability of the stall-controlled wind turbine at above-rated wind speeds (limiting power output), the power tended to fluctuate somewhat. The test results have been reported also in [77].

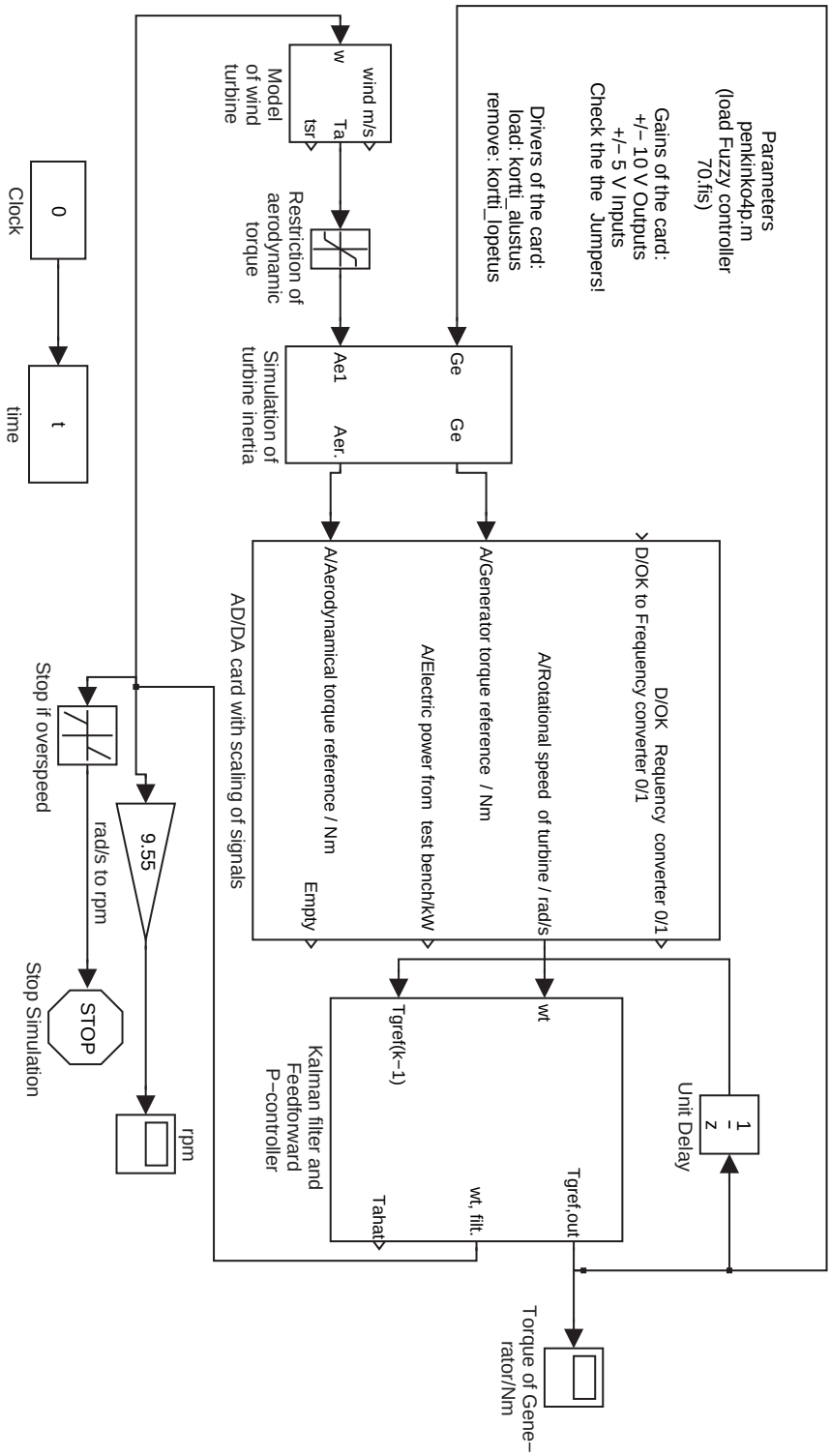

Figure 6.5: Simulink block diagram for control testing

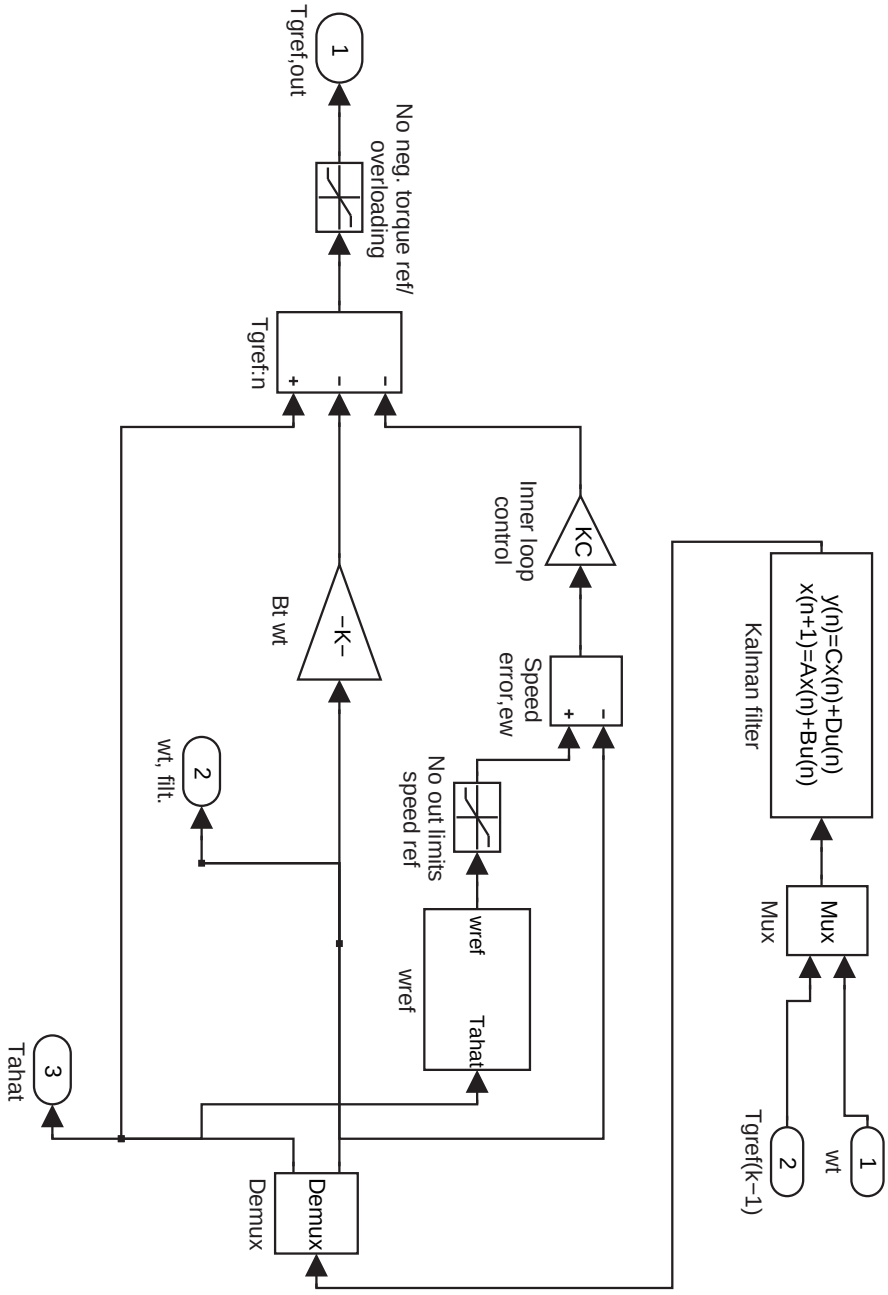

Figure 6.6: Simulink block for Kalman filter and rotational speed control loop (submodel for model in Fig. 6.5)

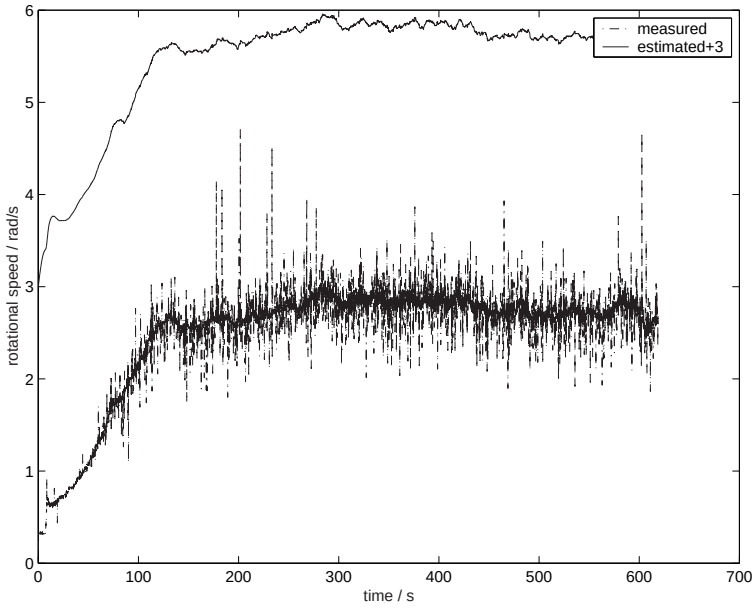

Figure 6.7: Measured and estimated rotational speed (shifted 3 rad/s for b/w printing)

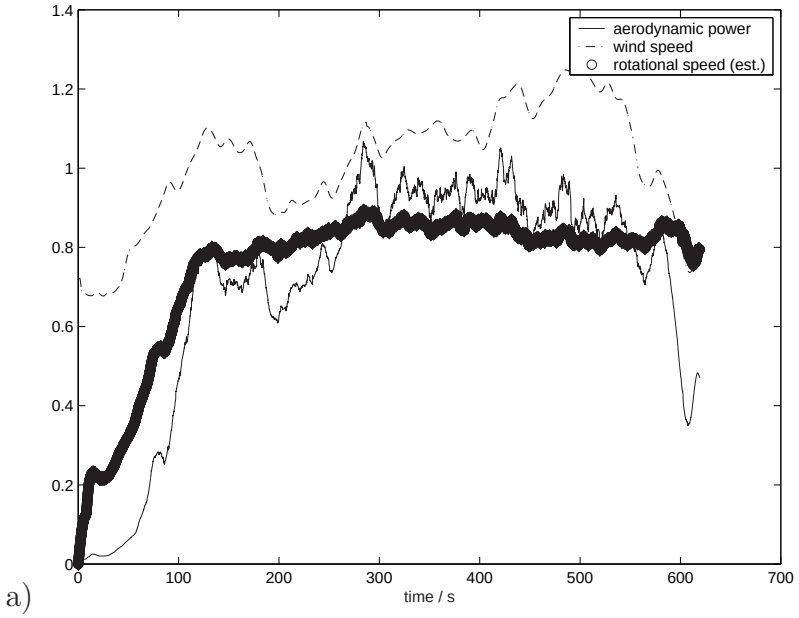

a)

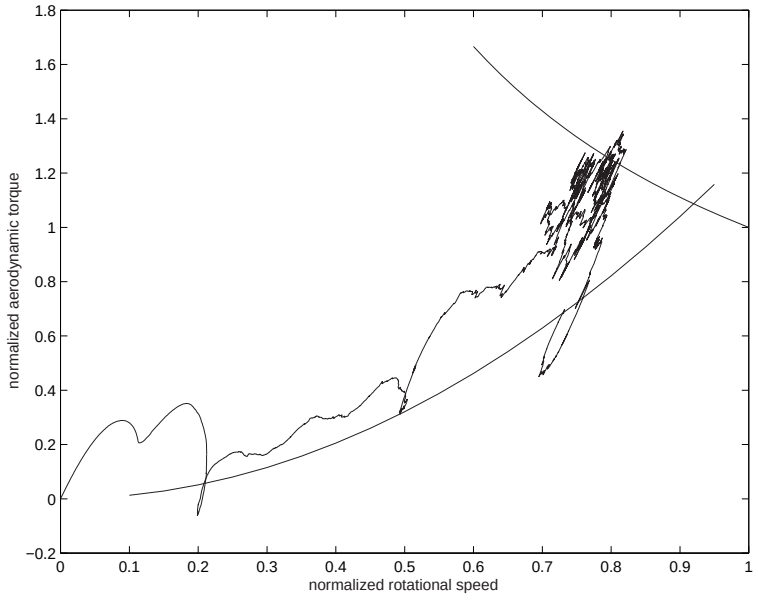

b)

Figure 6.8: a) Feed forward control, rated wind speed b) tracking on $\omega_t - T_a$ -plane; both figures normalized with rated values

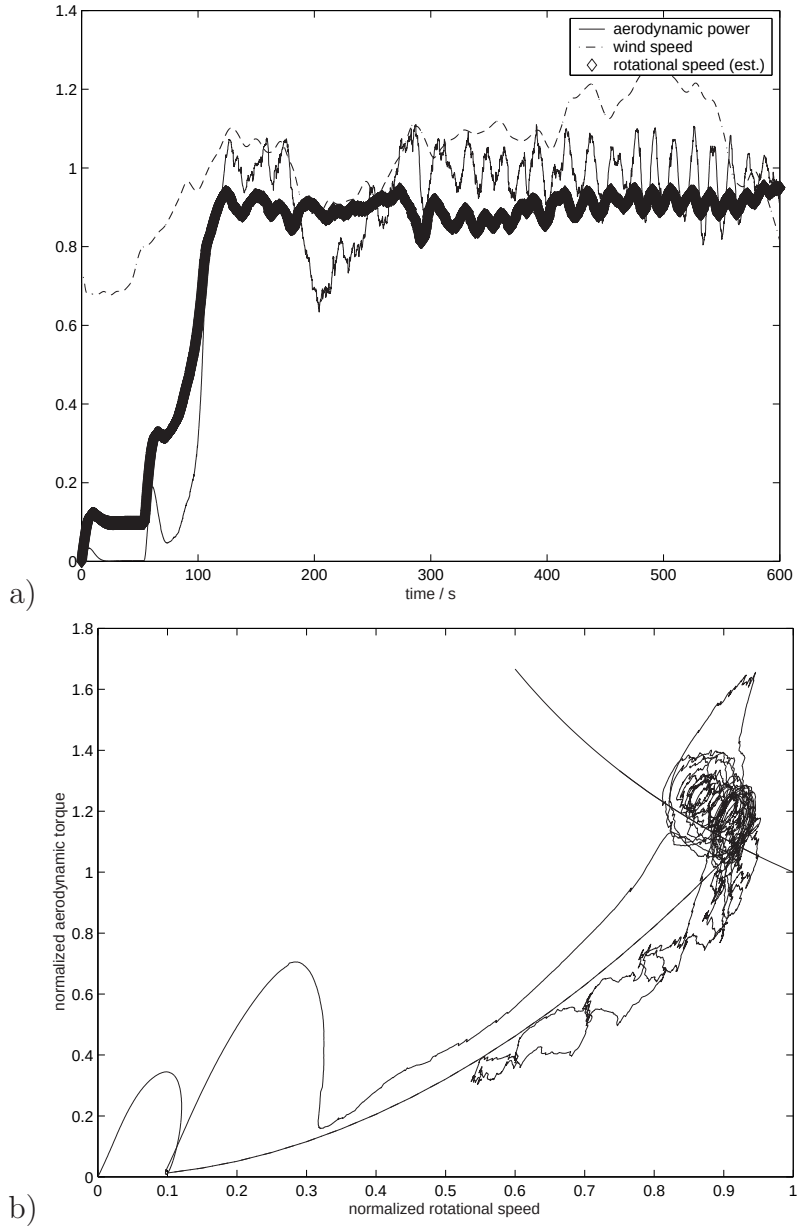

a)

b)

Figure 6.9: a) Fuzzy control, normalized with rated values, b) tracking on $\omega_t - T_a$ -plane, normalized with rated values

Chapter 7

Small scale wind turbine

7.1 General

In 1998, a small turbine was designed to charge batteries, and in 1999-2001 several prototypes of 300 W small permanent magnet generators were built [64], [65]. The small wind turbine was also built without pitch control, furling (turbine turning upwards), or eclipse (turbine turning sideways away from wind). The turbine had neither passive stall nor pitch control based on centrifugal forces or twisting blades, the solution being dictated by the turbine's mechanical simplicity and the durability requirements thereof. Instead, the plant's rotational speed was controlled and its power input limited by active means. Analogous to the large wind power drive, the rotational speed was controlled by a rectified generator current, and the power was fed into a battery as DC current, and thus a buck converter was used instead of a six-pulse grid inverter.

7.2 Description of test plant - realisation of controller

The control unit was governed by a microcontroller, an ATMEL AT90S8535 [3], containing a microprocessor, memory, analog to digital converter, pulse width modulation (PWM), and logic outputs. For compactness, the microcontroller was capable of controlling both current and rotational speed, which in the large drive were delegated to two separate computers. A reduced 8/16-bit accuracy also had to be taken into account.

The three-phase generator current was rectified with a six-pulse diode bridge (Fig. 7.1) and controlled by turning a field-effect transistor (FET) on

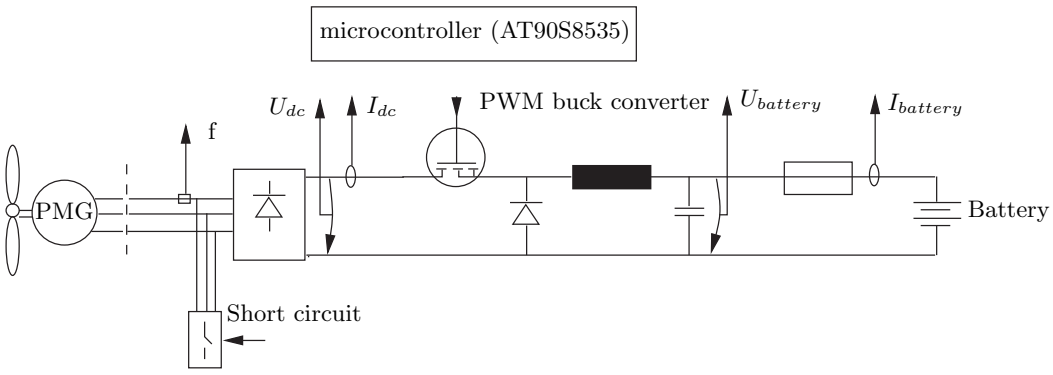

Figure 7.1: Circuit diagram of a small wind turbine controller

and off according to the PWM signal from the microcontroller. The pulsed current was then filtered with a low-pass filter, consisting of a series-connected coil and a parallel-connected capacitor. The control unit also had circuits to measure the turbine's rotational speed, the currents and voltages in the generator and battery plus the currents fed into two separate load circuits. For a more detailed description of the control unit design and programming, see [35].

Because of the buck converter topology as a step down DC converter, we could take control action only when the unloaded rectified generator voltage as subtracted twice from the diode step voltage exceeded the battery voltage. Since the nominal generator phase voltage unloaded was about 27 V at 550 rpm, and the battery voltage varied between 11-14 V, the rotational speed region controlled by the chopper showed a minimum of 150 rpm. However, at all speeds, the turbine could be halted by a relay between generator and diode rectifier, which short-circuited all the phases. Because of relatively high stator resistance, typical of small electrical machines, the short-circuit current was reduced to acceptable values.

Unlike in the large wind power drive, the commutation current was not an issue in the small wind power drive. In electrical machines below 10 kW, resistance is a dominating factor in phase impedance; consequently, the relation between rectified current and generator torque was linear throughout the operating envelope and verified with an external current probe and a torque transducer.

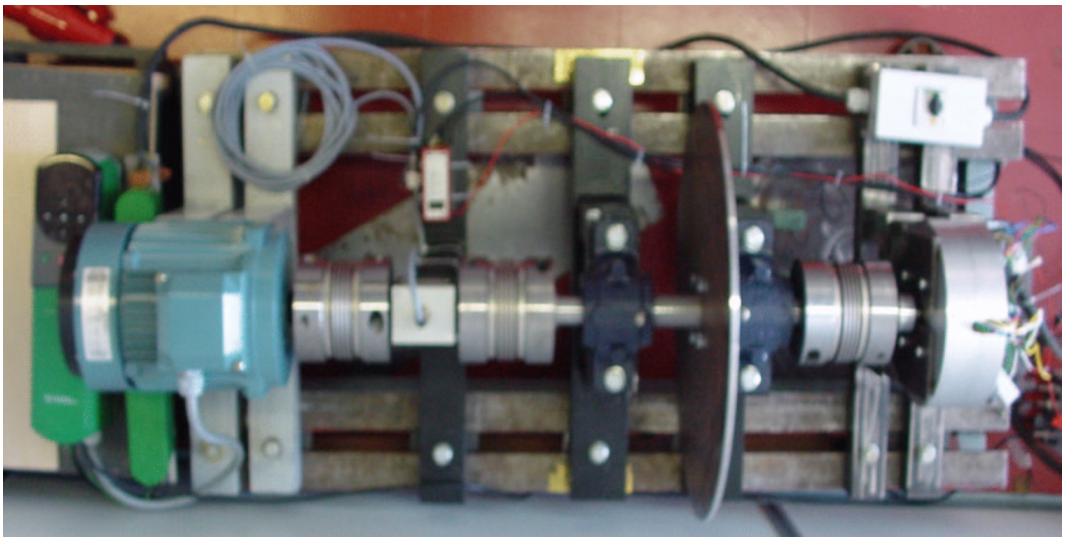

Figure 7.2: Small wind turbine test bench: From left to right: frequency converter, asynchronous motor, torque transducer, flywheel, and PMG

7.3 Test bench

The actual wind turbine was in the small drive test bench replaced by an asynchronous motor (1.1 kW, 980 rpm, 400 V), driven by a frequency converter Unidrive 1.5 kW (further details in Appendix B). Since rotational speeds and torques between motor and generator matched closely enough, the two were connected directly via a torque transducer and an iron flywheel, which simulated the inertia of a wind turbine (Fig. 7.2).

In Fig. 7.3, the frequency converter (FC) receives an aerodynamic torque reference $T_{a,ref}$ as an 0-10 V analog signal from the wind turbine model running on a PC in a MATLAB/Simulink environment. The model received a measured rotational speed and torque from the torque transducer with the signals galvanically separated. Because the Unidrive had a less sophisticated control algorithm than the ABB direct torque control in the ACS 600, the Simulink model controlled also measured aerodynamic torque to match the reference.

After the torque transducer, an iron plate was connected to the shaft with its inertia of 0.23 kgm^2 equivalent to the inertia of the test turbine. The 1.3 m diameter turbine had a greater inertia than usual because of being manufactured from an aluminium sheet. The test bench setup was at first used without any additional inertia, its own inertia being below 0.05 kgm^2. Consequently, the Kalman filter performed very poorly with the estimate of

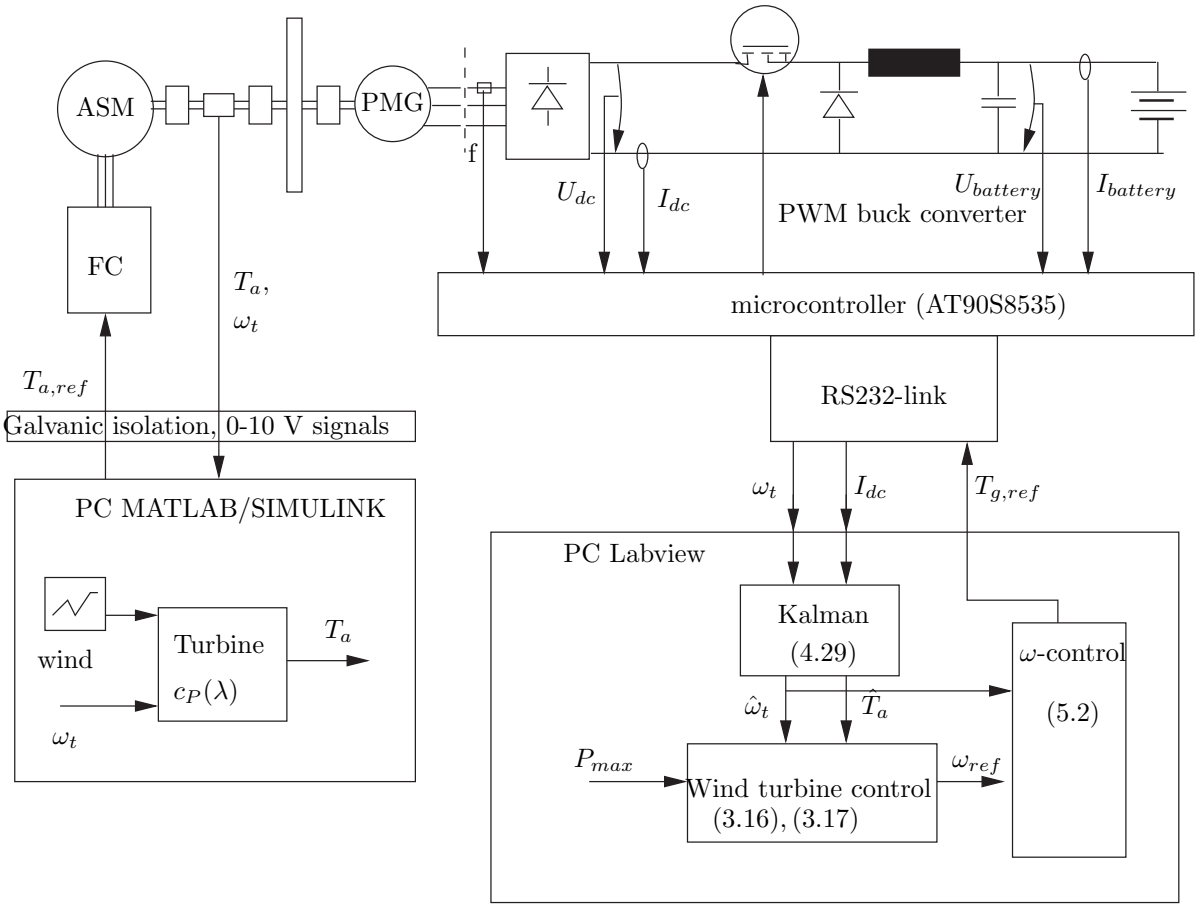

Figure 7.3: Layout diagram of a small test bench configuration

aerodynamic torque oscillating wildly perhaps due to the small eigenvalues of the Kalman matrix.

Tuning the Kalman filter parameters for system uncertainty and measurement noise, R_1 and R_2, respectively, proved time-consuming, as the multiplications were realized on the bit-shifting level (instead of, e.g., by multiplying directly by 3; the number byte was shifted by one bit to the left and the original number was added to the result). Because of the laborious tuning of the Kalman filter and the rotational speed controller parameters, these controllers were in later stages transferred into the PC Labview environment [50]. The values of the current rotational speed and the DC current were transferred through a serial port to a PC Labview model, which used equations (3.6)–(3.12); the current reference was then transferred back into the microcontroller (Fig. 7.3).

The Kalman filter parameters, the control parameter K_p, and the maximum power taken P_{max} could now be changed even during tests. Also the current values of the measured, estimated, and reference rotational speed were displayed in a graph as well as estimated aerodynamic torque and generator torque.

7.4 Bench tests

The wind turbine model was fed with measured and filtered wind speed. In MATLAB/Simulink, spatially filtered (as described in Section 4.1) wind speed was also fed into the model. We could thus see how well the control could follow the optimal tip speed ratio at below-rated wind speeds.

In the first runs, the rotational speed was clearly below the reference by about 50 rpm. The high seals friction resulted in 0.5 Nm of additional torque at 600 rpm and caused a gap between the reference and actual rotational speed. Thus the friction torque, $(B_{seals} + B_{bearings})\omega_t$, was subtracted from generator torque; the friction torque did not then brake the turbine twice, i.e., first in seals and then in the aerodynamic torque fed back into generator torque.

A third, intermediate region between below and rated wind speeds was included in the aerodynamic torque-reference speed curve. The wind turbine was operated in this region with a constant rotational reference of 600 rpm = 62.8 rad/s.

The output of the wind turbine could now be limited also to a certain value. On the Labview screen, the power could be commanded down to a certain value, as shown in Fig. 7.4, according to Eq. (3.11).

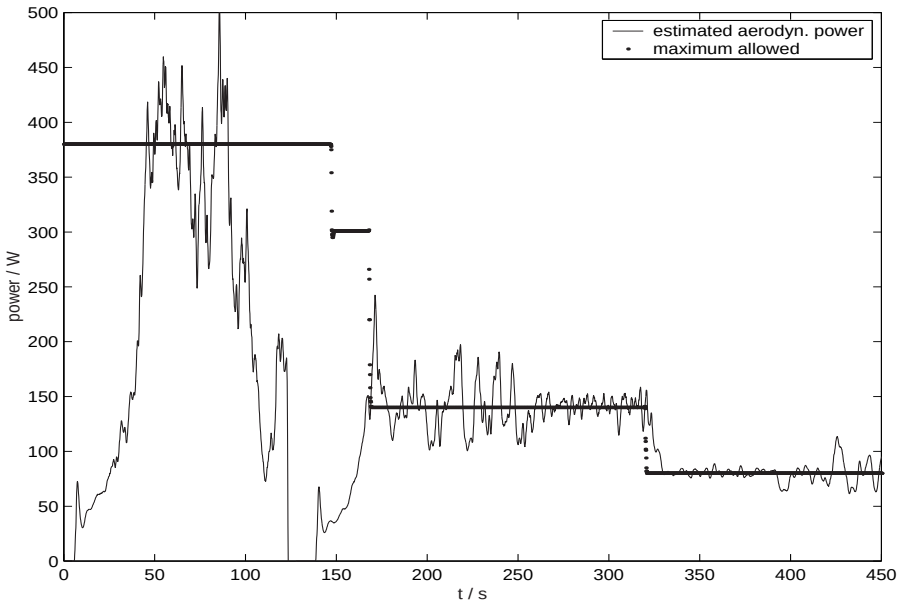

Figure 7.4: Power limitation in bench tests

7.5 Wind tunnel and field tests

The control unit and the turbine were tested in two wind tunnels. The first tests were run at the Institute of Energy Technology at TUT in an open-circuit wind tunnel, i.e., where the test chamber opens into a room space, and the air is sucked from the room at the front of the tunnel and blown through the test chamber. Because the cross section of the test chamber is a 1x1 m rectangle, the wind turbine with its 1.3 m diameter had to be placed behind the chamber (Fig. 7.5) with an additional diffuser placed after the tunnel. Although the airflow did not expand much coming out of the chamber, most of the turbine's swept area was covered with an about 1.1x1.1-m rectangle of airflow. The hub of the turbine was centered in the airflow from the tunnel. In this test, the turbine and the generator were mounted rigidly and did not turn during testing.

The controller was tuned during these tests, and the results show that it behaved well at both below- and above-rated wind speeds. The wind speeds were measured with a hand-held anemometer, indicating an even wind speed distribution all over the flow area, though the flow speed was somewhat less in a 20 cm wide area on the turbine's outer radius.

The wind turbine was tested later in a larger wind tunnel at the Laboratory of Aerodynamics at Helsinki University of Technology (Fig. 7.6). This

Figure 7.5: Wind turbine generator installed behind open end of wind tunnel at Energy Laboratory, TUT.

Figure 7.6: Wind turbine with tail vane, attached upside down in wind tunnel at Lab. of Aerodynamics, Helsinki University of Technology

wind tunnel is a 2x2 m rectangle with closed-loop air circulation. The test chamber ceiling shows a six-component scale to determine forces and torques on the tested turbine, and the turbine was mounted upside down on this scale (Fig. 7.7). The turbine configuration was complete with yaw bearings, slip rings to transfer power from the rotating part to the tower, and a tail to keep the turbine perpendicular to the wind.

Because we did not know the exact aerodynamic characteristics of the test turbine, we had to identify the turbine first. The wind speed was kept constant and the rotational speed was changed stepwise. Torque and the produced power were measured at each rotational speed. The test was repeated at wind speeds of 5-10 m/s to eliminate the effects of different Reynolds numbers and air compression between turbine and tunnel walls. The compression has more effect at higher rotational speeds as the solidity of the turbine increases and the air has to flow more between the turbine and the wall of the tunnel.

The values of k_T and k_ω were determined with Eqs. (3.4) and (3.6) from the maximum power at each wind speed. The optimum k_ω value was about 29, though the optimal area was wide. It is desirable to rotate the turbine at a slightly higher than optimal speed, for the turbine acts then more at its optimal tip speed ratio during gusts and has extra rotational energy during

Figure 7.7: Running wind turbine, windward side. On ceiling, 6-component scale clearly visible where turbine is mounted.

a flaute. Therefore the k_ω value was set at 32.

In the second test, we tested the rotational speed control loop. The rotational speed reference was increased stepwise from 15 to 65 rad/s, and after reaching the speed, it was driven stepwise back to 15 rad/s, while the air speed was kept at 8 m/s. The rotational speed showed some vibration around the reference, as seen in Fig. 7.8 (K_p=0.2). Note, however, that the control should cope under normal operating conditions when the rotational speed reference does not change so rapidly.

As these values were fed into the controller, the plant's operation was tested at below-rated speeds. The turbine behaved well, considering that the wind speed in the tunnel could not be changed abruptly due to the turbine's rotating propeller masses and the circulating air mass. At below-rated wind speeds, the turbine maintained its rotational speed nearly at optimum.

Finally, the control was tested in the most demanding region, at above-rated wind speeds, varied between 8-14 m/s. The feedback constant of the rotational speed control, K_p, had a value of 0.05. However, this was too small to hold the rotational speed to its reference. As we can see in Fig. 7.9, the turbine overspeeded at 60 s. The value of K_p was set back to 0.2, resulting in satisfactory behavior at above-rated speeds and switching between them. The estimated aerodynamic power was also kept within limits, as shown in Fig. 7.10.

Lastly, we studied the behavior of a braked generator. The generator was

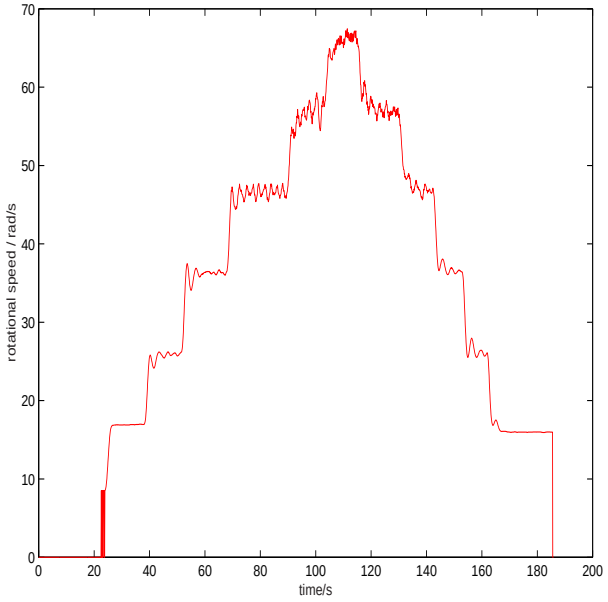

Figure 7.8: Rotational speed control loop test

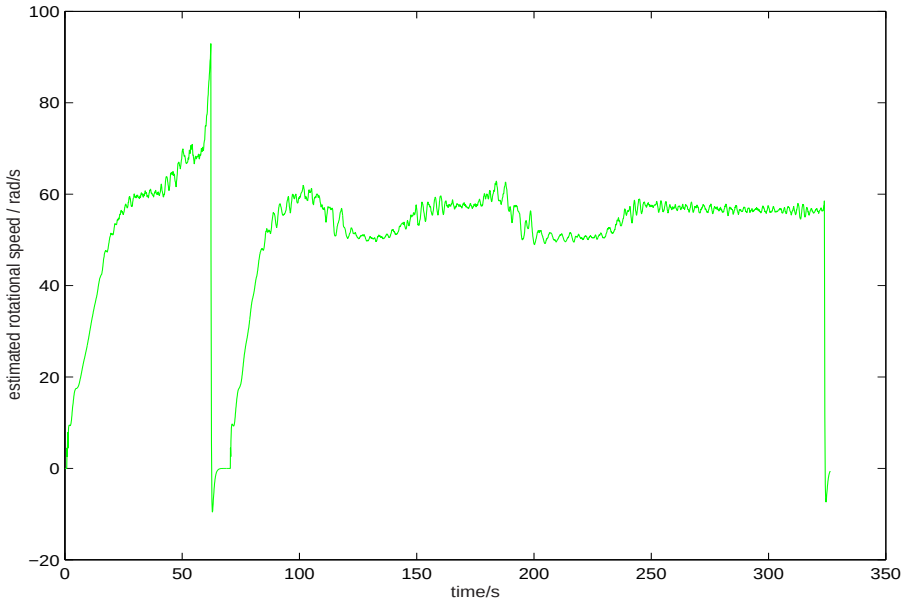

Figure 7.9: Estimated rotational speed as air speed was varied between 8-14 m/s

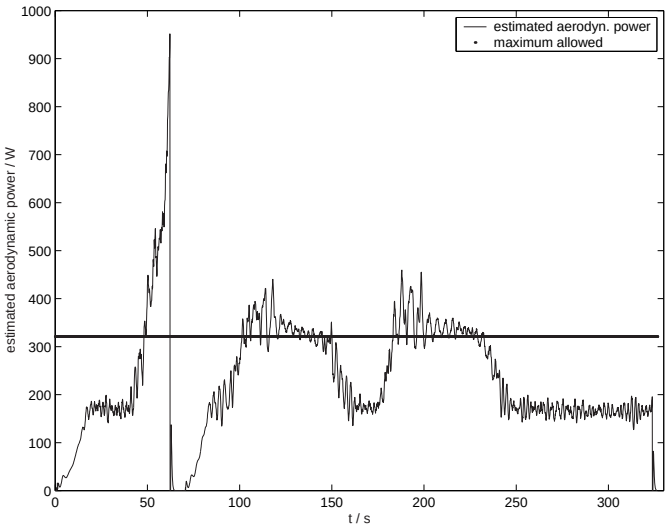

Figure 7.10: Estimated aerodynamic power in the previous situation

short-circuited by a relay in the control unit, and the air speed was increased in the wind tunnel. At above 20 m/s, the turbine vibrated considerably, and the tests were not continued beyond 25 m/s. As in field tests we did not observe vibration at the same speeds, we assume it was caused by interaction between tunnel wall and turbine.

7.6 Field tests

For a month and a half, from December 4, 2000 to January 15, 2001, the wind turbine was tested on the roof of the TUT Radio Club. The turbine was erected between a radio mast and a satellite antenna, and the electronics developer worked three floors below the turbine, where the cables from turbine and anemometer were run. However, winds were quite weak on the roof because of the nearby tall buildings and forest.

In the end, the wind turbine was tested in field conditions on a remote island in the Finnish archipelago. The turbine was located on a rocky hill, rising steeply from the sea. The site was open to winds from degrees 90-270 in compass rose, i.e. for the east, south and west winds. The control box and batteries were located about 100 meters away in a cabin. The wind speed, directions, temperature etc. were measured with a Davis Instruments Monitor II logging device [17].

The control parameters were tuned in an approximate manner, and the

Figure 7.11: Wind turbine on a remote island in January, 2001. Note anemometer and wind vane beneath turbine.

turbine started at a wind speed of about 3 m/s and ran smoothly. However, the wind conditions were too light during the test period of January 25-28, 2001, for testing control performance at above-rated wind speeds. As we had not yet implemented logging via a serial port, we have no log curves to show.

7.7 Discussion

For laboratory experiments, the small wind turbine was in many ways more suitable than the large machine, for its parts were cheaper and it could be manufactured in two months compared to a year for the larger generator. The smaller turbine could be handled by one person, and the generator voltage

was lower, causing less risk of electrical shocks. Furthermore, we had a much lower damage risk during overspeeding. In addition, tests can be carried out in an ordinary office room, whereas a laboratory hall was needed for the large generator.

In test bench and wind tunnel experiments, we encountered aerodynamic, electro-mechanical, and electronics problems, for though the microcontroller is widely used in everyday products, it was not very adaptable for continuous re-coding especially when the assembly language was used. A computationally light code must be written at the cost of clarity, and even that is prone to error. Transferring the control system into Labview for tuning and logging variables resulted in a more rapid tuning of the system.

The bearings of the flywheel, which simulated turbine inertia, had large rubber seals and resulted in high damping, B_t. Vibration was thus effectively damped in bench, but the Kalman filter had to be re-tuned in the wind tunnel as hunting returned.

The below-rated speed region was not an issue because the plant was stable and because the turbine had a relatively wide high-efficiency area in the $c_P(\lambda)$ -curve. Rather, time was mostly spent in stabilizing the turbine in the above-rated power area, where the power had to be limited. Due to the inherent instability of the wind turbine, + 15% / -10% vibration remained around the rated power. As the maximum power was lowered, also vibration diminished considerably.

The wind tunnel experience underlines the importance of estimating accurately the noise (R_1) and measurement error (R_2) matrices. This fact is rarely mentioned in textbooks, where the matrices are given and simulation examples behave well. In this application, the control loops were nested, and despite different time scales in each loop, vibration and hunting spread throughout the system. Mäkilä [41] viewed these matrices as design parameters in LQG control.

In addition, it was very important not to let the turbine overspeed at above-rated wind speeds, for then the aerodynamic torque exceeded the maximum allowed generator torque and the turbine had to be stopped by short-circuiting.

Chapter 8

Conclusions

Both controllers presented here, feedforward and fuzzy, could stabilize a large wind power drive in laboratory tests. The feedforward controller was also able to stabilize a small wind power drive in laboratory tests, wind tunnel, and field conditions. This proves that the variable speed, fixed pitch (VSFP) wind turbine is still a viable alternative despite the advent of variable pitch machines. The nonlinear dynamics of the VSFP turbine can be governed by the feedforward control method and an advanced estimator, the Kalman filter.

Use of feedforward control simplifies the control design of the VSFP turbine, since only a simple proportional controller without parameter scheduling is required for the turbine's whole operating envelope. The Kalman filter proved an effective tool in delivering an accurate estimate of aerodynamical torque and rotational speed. It was also shown how vital an estimate of aerodynamic torque, supplied by the Kalman filter, is for the fuzzy controller.

Limiting the power output well below rated also was tested successfully with the small wind power plant in laboratory and wind tunnel. The output could be restricted from 300 W down to 50 W. This demonstrated how three outputs—generator torque, rotational speed, and power output—can be controlled by the generator current alone.

There is a theoretical flaw in estimating aerodynamic torque; that is, that it is assumed to be an independent disturbance. In reality, there is a dependency, though uncertain, on aerodynamic torque from rotational speed. In practice, this flaw did not affect the accuracy of estimation.

The feed-forward and fuzzy controllers were first tuned by simulation and then in a test bench. During tuning, the structure of the controller with its several inner loops is exposed. A rapid control action in generator torque in the inner loops induces reference fluctuation in the outer loops, which in turn increases fluctuation in the inner loops. The fuzzy controller was defined

easily, but tuning the low-order controller we used was labor-intensive.

A microcontroller-based control unit was built for the smaller controller. Because of the coding of the assembly language, tuning the parameters of the small wind turbine controller proved very time consuming. The parameters were written in assembly code instead of variables or memory locations, and therefore the higher level control loops were transferred to PC Windows/Labview for quicker tuning.

8.1 Further research

We will conduct some more wind tunnel and field tests on the small wind turbine to ensure and report wind turbine behavior in the whole operating envelope. The effect of the stall-delay phenomenon must also be simulated and tested.

The feed-forward controller presented here must be compared with one tuned with LQG-rules. A compromise will also have to be made between higher energy yield and lower fatigue (due to less aggressive control actions). Furthermore, a robust controller will be designed.

An idea has been entertained to develop a fuzzy controller, self-tuned by neural networks, whereby a single turbine could adapt itself to conditions on different sites and changes in plant parameters [61]. Self-tuning can also be studied with classical controllers.

In a more distant future, a feed-forward controller may also be implemented in a wind turbine with pitch control. Such a configuration, however, will involve the problematics of multiple input multiple output control.

Bibliography

[1] Vestas 660 kW wind turbine. Company brochure.

[2] ABB. Ohjelmointiopas: ACS 600 -taajuusmuuttajat 2,2-630 kW [in Finnish; Programming manual, ACS 600 frequency converters]. ABB Industry Oy, 1997.

[3] Atmel. AT90S/LS8535 AVR Microcontroller Data Sheet. http://www.atmel.com.

[4] A. Betz. Wind-Energie und ihre Ausnutzung durch Windmuehlen. Vandenhoeck et Ruprecht, Göttingen, 1926.

[5] J. Blix. Another 3 MW unit - windformer; development projects from a utility point of view. In P. Helm and A. Zervos, editors, European Wind Energy Conference 2-6 July 2001, Copenhagen: Wind Energy for the New Millennium, volume 1 of Proceedings of the European Wind Energy Conference 2-6 July 2001, Copenhagen, Denmark, pages 166–168, Jan 2002.

[6] G. Böhmeke, R. Boldt, and H. Beneke. Direct drive, geared drive, intermediate solutions - comparison of design features and operating economics. In R. Watson, editor, European Wind Energy Conference '97, pages 664–667. European Wind Energy Association, Irish Wind Energy Association, 1998.

[7] P. Bongers, W. Bierbooms, S. Dijikstra, and T. van Holten. An integrated dynamic model of a flexible wind turbine. Technical report, Delft University of Technology, 1990.

[8] P. M. Bongers. Modeling and Identification of Flexible Wind Turbines and a Factorizational Approach to Robust Control Design. PhD thesis, Delft University of Technology, June 1994.

[9] B. Bose (ed.). Power electronics and variable frequency drives. IEEE 1996. IEEE Press, New York, 1996.

[10] I. Buehring et al. Control policies for wind energy conversion systems. IEE-Proc. C, 128(5), 1981.

[11] R. Cardenas-Dobson and G. Asher. Power limitation in variable speed wind turbines using pitch control and a mechanical torque observer. Wind Engineering, 20(6):363–387, 1996.

[12] R. Cardenas-Dobson, G. Asher, and G. Asher. Torque observer for the control of variable speed wind turbines operating below rated wind speed. Wind Engineering, 20(4):259–285, 1996.

[13] B. Connor, W. Leithead, , and A. Mercer. Dynamics and control of a flexible wind turbine with a coning rotor. In A. Zervos, H. Ehmann, and P. Helm, editors, Proc. of European Union Wind Energy Conference '96, volume 1, pages 878–881. H.S. Stephens & Associates, May 1996.

[14] B. Connor and W. Leithead. Control strategies for variable speed stall regulated wind turbines. In Proc. of European Wind Energy Conference '94, 1994.

[15] B. Connor and W. Leithead. Investigation of control strategy for RES 1 MW variable speed wind turbine. Technical report, Univ. of Strahclyde, UK, 1996.

[16] B. Connor, W. Leithead, and S. Robertson. Robust two-level control design approach to variable speed stall regulated wind turbines. In R. Watson, editor, European Wind Energy Conference '97, pages 551–554. European Wind Energy Association, Irish Wind Energy Association, 1998.

[17] Davis Instruments Corp. Weather Monitor II: Owner's manual, April 2000. Prod. nro 7440.

[18] D. Eggleston and F. Stoddard. Wind Turbine Engineering Design. Van Nostrand Reinhold, New York, 1983.

[19] T. Ekelund. Control of variable speed wind turbine in a broad range of wind speeds. Technical Report No. 1721, School of Electrical and Computer Engineering, Chalmers Univ. of Technology, Göteborg, Sweden, 1994.

[20] T. Ekelund. Modeling and linear quadratic optimal control of wind turbines. PhD thesis, School of Electrical and Computer Engineering, Chalmers University of Technology, Göteborg, Sweden, 1997.

[21] J. Ernst-Cathor. Drehzahlvariable Windenergieanlage mit Gleichstromzwischenkreis-Umrichter und Optimum-suchendem Regler. PhD thesis, TU-Braunschweig, Dec 1986.

[22] E. M. Fateev. Windmotors and Wind Power Stations. Moscow, 1948.

[23] L. Freris (ed.). Wind Energy Conversion Systems. Prentice Hall, Englewood Cliffs, N.J., 1989.

[24] R. Gasch (ed.). Windkraftanlagen: Grundlagen und Entwurf. B.G. Teubner, Stuttgart, 2 edition, 1993.

[25] T. Glad and L. Ljung. Control Theory: Multivariable and nonlinear methods. Taylor & Francis Group, London, 2000.

[26] A. Grauers. Synchronous generator and frequency converter in wind turbine applications: system design and efficiency. Chalmers Univ. of Technology, 1994. Lic. Thesis.

[27] M. S. Grewal and A. P. Andrews. Kalman filtering: theory and practice. Prentice-Hall Inc., 1993.

[28] E. Haapanen. Tuulesta temmattua [in Finnish; Some issues about wind power]. Technical Report 2a, Ins. tsto Erkki Haapanen Ky, Raininkaistetie 27, 35600 Halli, Jan 2001. 14 pp.

[29] Humusoft. RealTime Toolbox, v. 3.0: User's Manual. www.humusoft.cz.

[30] Humusoft. AD 512 Data acquisition card: User's manual. http://www.humusoft.cz, 1997. 16 p.

[31] M. T. Iqbal, A. Coonick, and L. Freris. Some control aspects of wind turbine. In IEE Colloquium on Two Decades of Fuzzy Control, volume 1, 1993.

[32] R. E. Kalman. A new approach to linear filtering and prediction problems. Transactions of the ASME–Journal of Basic Engineering, 82(Series D):35–45, 1960.

[33] H. Keppola, R. Perälä, L. Söderlund, and H. Vihriälä. Preliminary test results of an axial flux toroidal stator wind power generator. In Proc. of ICEM 2000: International Conference on Electrical Machines, 28-30 August 2000, Espoo, Finland, volume 3, pages 1480–1484. ICEM 2000 Secreteriat, 2000.

[34] H. Keppola, R. Perälä, H. Vihriälä, P. Puttonen, and L. Söderlund. A gearless wind power drive:
part 1: Static test results. In P. Helm and A. Zervos, editors, European Wind Energy Conference 2-6 July 2001, Copenhagen: Wind Energy for the New Millennium, volume 1 of Proceedings of the European Wind Energy Conference 2-6 July 2001, Copenhagen, Denmark, pages 1086–1089, Jan 2002.

[35] J. Kriikka. Pientuulivoimalan säädin [Control unit of a small wind turbine; in Finnish]. Master's thesis, Tampere Univ. of Technology, Dept. of Electrical Engineering, June 2001. 60 p.

[36] W. Leithead and C. B. Control of variable speed wind turbine with induction generator. In Proc. of Control '94, Warwick, March 1994.

[37] W. Leithead, S. de la Salle, and D. Readon. Wind turbine control objectives and design. In European Community Wind Energy Conference, Madrid, pages 510–515, Sep 1990.

[38] W. Leithead, S. de la Salle, and D. Reardon. Role and objectives for control of wind turbines. IEE Proc-C, 138(2):pp. 135–148, 1991.

[39] W. Leonhard. Control of Electrical Drives. Springer-Verlag, 1984.

[40] P. Madsen and S. Frandsen. Pitch angle control for power limitation. In Proceedings of European Wind Energy Conference '94, Hamburg, 1984.

[41] P. M. Mäkilä. Linear quadratic control revisited. Automatica, 36:83–89, 2000.

[42] I. Mathworks. Using Matlab 5.2. 24 Prime Park Way, Natick, MA 01760-1500, 1998.

[43] I. Mathworks. Using Simulink 2.0. 24 Prime Park Way, Natick, MA 01760-1500, 1998.

[44] A. S. Mercer and E. Bossanyi. Stall regulation of variable speed hawts. In A. Zervos, H. Ehmann, and P. Helm, editors, Proc. of the European Union Wind Energy Conference '96, pages 825–828. H.S. Stephens & Associates, May 1996.

[45] D. Millborrow and L. Harrison. The windicator - quaterly table of global wind capacity. Wind Power Monthly, 18(1):50, Jan 2002. ISSN 0109-7318.

[46] J. Mokka. Vaihtelevanopeuksisen tuulivoimakäytön mallintaminen [in Finnish: Modeling of variable speed wind power drive]. Master's thesis, Tampere Univ. of Electricitry, Dept. of Electrical Engineering, Tampere, Finland, Nov 1997. 99 p.

[47] Morthorst. Special topic course on wind engineering. Course material, May 1998. VTT, Espoo, Finland.

[48] P. Mutschler, B. Hagenkort, and S. Jöckel. Control method for variable speed stall controlled wind turbines. In R. Watson, editor, European Wind Energy Conference '97, pages 542–545. European Wind Energy Association, Irish Wind Energy Association, 1998.

[49] N.N. Lagerwey windturbine bv, lagerwey 50/750. Company Brochure. Hanzeweg 31, P.O. Box 279, Barneveld, the Netherlands.

[50] N.N. National Instruments, Labview: User's Manual, 1999.

[51] N.N. Jeumont industrie and wind energy. Company Brochure, Jun 2001.

[52] N.N. Winwind oy. Company WWW-site, 2002.

[53] P. Novak. On the modelling and partial-load control of variable speed wind turbines. Technical Report 2061, Control Engineering Laboratory, School of Electrical and Computer Engineering, Chalmers University of Technology, Göteborg, Sweden, Aug 1995. ISBN 91-7197-170-X.

[54] P. Novak, T. Ekelund, I. Jovik, and B. Schmidtbauer. Modeling and control of variable speed wind turbine drive-system dynamics. IEEE Control Systems, 15(4):28–38, Aug 1995.

[55] R. Peltonen. A numerical method for analysis and design of airfoils in subsonic flow. Series a, Helsinki University of Technology, Espoo, Finland, October 2000.

[56] R. Perälä. Design of an Axial Flux Permanent Magnet Wind Power Generator. Tampere University of Technology, Dept. of Electrical Engineering, Tampere, Finland, 1998. Lic. Thesis.

[57] PRElectronic, Lerbakken 10, Rønde, Denmark, http://www.prelectronics.com. 2255, fI-Ff converter. No. 2255V100-IN(9913).

[58] P. Puttonen. Comparison of current-source frequency converters applicable for wind power application [Tuulivoimakäyttöön soveltuvien virtavälipiirillisten taajuudenmuuttajien vertailu, in Finnish]. Technical report, Tampere Univ. of Technology, Inst. of Power Electronics, 2001. Lic. Thesis.

[59] P. Puttonen, M. Salo, and H. Tuusa. Experimental results of a 100 kW current-source PWM-converter operation with a multipole permanent magnet synchronous generator for a variable speed wind energy drive. In Proceedings of the Sixth European PCIM 2000 / POWER QUALITY Conference, Nürnberg, Germany, June 6-8 2000.

[60] P. Ridanpää. Fuzzy control of a wind power plant. M.Sc. thesis, Tampere University of Technology, Dept. of Electrical Engineering, Tampere, Finland, Tampere, February 1998.

[61] P. Ridanpää, H. Vihriälä, and L. Söderlund. Reducing cost of wind energy by self-tuning controller. In E. Petersen et al., editor, 1999 European Wind Energy Conference and Exhibition, Nice, France, March 1-5, 1999, volume 1, pages 873–876, 1999.

[62] P. Ridanpää, H. Vihriälä, L. Söderlund, J. Syrjärinne, and J. Saarinen. Modelling of fuzzy controlled variable speed, stall regulated wind turbine. In M. Hamza, editor, Modelling and Simulation, Proceedings of the IASTED International Conference on Modelling and Simulation, May 13-16, 1998, Pittsburgh, Pennsylvania, USA, pages 200–204, Anaheim, 1998. IASTED/ACTA Press.

[63] D. Robb. Model based predictive control with application to renewable energy systems. PhD thesis, University of Stratclyde, Industrial Control Centre, Garrad Hassan Partners, Kelvin Science Park, Glasgow, March 2000. Advisor: William Leithead.

[64] T. Rovio. Pientuulivoimalan generaattorin suunnittelu [The design of a small-scale wind power generator; in Finnish]. M.Sc. thesis, Tampere Univ. of Technology, Dept. of Electrical Engineering, Dec 2000. 95 p.

[65] T. Rovio, H. Vihriälä, L. Söderlund, J. Kriikka, and M. Hyppönen. Axial and radial flux generators in small-scale wind power production. In P. Helm and A. Zervos, editors, European Wind Energy Conference 2-6 July 2001, Copenhagen: Wind Energy for the New Millennium, volume 1 of Proceedings of the European Wind Energy Conference 2-6 July 2001, Copenhagen, Denmark, pages 1094–1097, Jan 2002.

[66] Siemens. IL300 Linear optocoupler, datasheet.

[67] M. Simoes, B. Bose, and R. Spiegel. Fuzzy logic based intelligent control of a variable speed cage machine wind generation system. IEEE Trans. on Power Electronics, 12(1):87–95, 1997.

[68] SKS-Automaatio. Tekel Pulssianturit [in Finnish; Tekel pulse encoders]. http://www.sks.fi. N:o 733261.

[69] L. Söderlund, J.-T. Eriksson, J. Salonen, H. Vihriälä, and R. Perälä. A permanent-magnet generator for wind power applications. IEEE Transactions on Magnetics, 32(4):2389–2392, 1996.

[70] L. Söderlund, A. Koski, H. Vihriälä, J.-T. Eriksson, and R. Perälä. Design of an axial flux permanent magnet wind power generator. In Proceedings of Eighth International Conference on Electrical Machines and Drives, Cambridge, UK 1-3 September 1997, number 444, pages 224–228. IEE, 1997.

[71] E. Spooner and B. Chalmers. "TORUS", A slotless, toroidal-stator, permanent magnet generator. IEE-Proceedings-B, 139(6):497–506, November 1992.

[72] B. E. Systems. Active stall system. Sales Brochure, Denmark, 1998.

[73] B. Tammelin. Finnish Wind Atlas [Suomen tuuliatlas]. Finnish Meteorological Institute, 1991. 356 p.

[74] H. Vihriälä. Permanent magnet generator in wind power plant. Master's thesis, Tampere Univ. of Technology, Dept. of Electrical engineering, Tampere, Finland, 1994. (in Finnish).

[75] H. Vihriälä. Control of a Variable Speed Wind Turbine. Tampere University of Technology, 1998. Licentiate Thesis, Available: *http* : *//helium.ee.tut.fi/weg_articles/windpowerart.html*.

[76] H. Vihriälä. Pientuulivoimalan säätö [Control of a small wind power plant; in Finnish]. Internal report, Lab. of Electromagnetics, June 1999.

[77] H. Vihriälä, R. Perälä, P. Mäkilä, and L. Söderlund. A gearless wind power drive: part 2: Performance of control system. In P. Helm and A. Zervos, editors, European Wind Energy Conference 2-6 July 2001, Copenhagen: Wind Energy for the New Millennium, volume 1 of Proceedings of the European Wind Energy Conference 2-6 July 2001, Copenhagen, Denmark, pages 1090–1093, Jan 2002.

[78] H. Vihriälä, R. Perälä, L. Söderlund, and J.-T. Eriksson. Reducing costs of wind power with a gearless permanent magnet generator. In H. Vihriälä, T. Toppila, M. Pihlatie, E. Peltola, and H. Holttinen, editors, Proceedings of EWEA Special Topic Conference '95: The Economics of Wind Energy, 5th-7th September 1995, Helsinki, Finland, volume 1, pages 225–229, Espoo, Finland, 1996. Finnish Wind Power Asscoation.

[79] H. Vihriälä, P. Ridanpää, R. Perälä, and L. Söderlund. Control of variable speed wind turbine with feedforward of aerodynamic torque. In E. e. a. Petersen, editor, 1999 European Wind Energy Conference and Exhibition, Nice, France, March 1-5, 1999, volume 1, pages 881–884, 1999.

[80] H. Vihriälä, P. Ridanpää, and L. Söderlund. Control of variable speed, stall regulated wind turbine: Comparison between adaptive and fuzzy controller. In R. Watson, editor, European Wind Energy Conference '97, Dublin, pages 559–563, Slane, Country Meath, Reb. of Ireland, Jan 1998. European Wind Energy Association, Irish Wind Energy Association. Available: $http://helium.ee.tut.fi/weg\_articles/windpowerart.html$.

[81] A. Wobben. Oral presentation. 22.5.1996 in the European Union Wind Energy Conference '96, Göteborg, Sweden.

[82] S. Øye A.F.M. Unsteady wake effects caused by pitch angle change. Technical report, Univ. Of Denmark, 1986.

[83] L. Zadeh. Fuzzy sets. Information Control, 8(3):338–353, 1968.

[84] G. Zhang and J. Furusho. Control of robot arms using joint torque sensors. IEEE Control Systems, pages 48–54, February 1998.

Appendix A

Data of the large test bench

radius of the simulated turbine R=10 m
air density $\rho = 1.26$ kg/m^3)
Driving Motor: 250 kW, 992 rpm, 400 V, manufactured by ABB Motors Oy, Vaasa
5:1 chain transmission between motor and generator
$J_{t,sim} = 27\ 000$ kgm^2
Motor driven by ABB ACS 600 Frequency converter
Permanent magnet generator: 100 kW, 60 rpm, 360 V, Designed and manufactured by Tampere Univ. of Technology/Inst. of Electromagnetics
Outer Diameter 2.5 m

Appendix B

Data of the small test bench

Generator: 300 W, 550 rpm, 50 V,
Motor ABB 1,5 kW, 980 rpm, 400 V
Frequency converter (for the asynchronous motor) Unidrive 1,5 kW, 400 V
Torque transducer: Hottinger T20WN/200Nm
Flywheel inertia: 0.23 kgm^3